DISSOLUTION KINETICS OF VOLCANIC ASH

Undergraduate Research Thesis
Submitted in partial fulfillment of the requirements for graduation
with research distinction in Earth Sciences
in the undergraduate college of Arts and Sciences
At The Ohio State University

By

Lillian R. Kleban
The Ohio State University
2020

Approved by

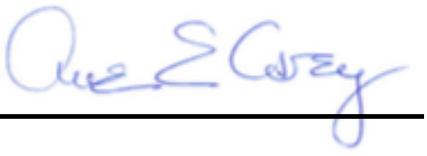

Dr. Anne E. Carey, Advisor
School of Earth Sciences

TABLE OF CONTENTS

ABSTRACT

Over geologic timescales CO_2 in the atmosphere is greatly affected by the weathering of silicate and phosphate rocks. Weathering of Ca-Mg phases is important because it results in precipitation of Ca Mg carbonates and removal to marine sediments, thereby affecting long term CO_2 uptake. Weathering of iron or phosphate phases is important because these reactions release nutrients that promote plant growth and take up CO_2 as organic carbon in the short term. This project investigates the dissolution kinetics of volcanic ash from five different eruptions (Mount St. Helens, USA eruption; Mt. Pinatubo, Philippines eruption; Eyjafjallajökull, Iceland; Mt. Pacaya, Guatemala; and Tungurahua, Ecuador eruptions) in synthetic sea water and in freshwater solutions, with and without the addition of iron oxidizing bacteria. Bulk ash composition determined by x-ray fluorescence ranged from basaltic andesite, to trachy-andesite, andesite and trachydacite. X-ray diffraction indicates the presence of plagioclase in all samples although the compositions both within ash and among samples could vary substantially. Over the course of the experiment, the solutions were sampled periodically via syringe, filtered, and analyzed with a Skalar San++ nutrient analyzer to determine concentrations of silica and phosphate. Marine experiments spanned 834 days. Freshwater experiments spanned 578 days. On the first day of the freshwater experiments, approximately 0.5 ml of *Sideroxydans lithotrophicus* in growth media was added to one set of the freshwater duplicates. Equal amounts of *Mariprofundus ferrooxydans* in growth media was added to one set of marine duplicates 260 days into dissolution experiments. Samples were also analyzed for iron by use of the ferrozine method; however, the concentrations of iron were too low to be detected (LOD=3 ppb). Phosphate concentrations were close to the detection limit and varied over time.

The silica concentrations increased gradually over time and dissolution rates were estimated from a linear fit of the data. Samples with or without bacteria exhibited similar rates based on Si dissolution. When normalized for specific surface area, the highest dissolution rate was from the 2010 eruption of Pacaya, which had basaltic-andesitic composition. The initial silica release rate in freshwater without bacteria was $7.8 \cdot 10^{-12}$ mole Si/m^2/s, and in artificial seawater: $3.5 \cdot 10^{-12}$ mole Si/m^2/s. In general, marine dissolution rates were of the same order of magnitude as freshwater release rates, but slightly slower. The lowest release rate was $1.5 \cdot 10^{-12}$ mol Si /m^2 /s, from Icelandic ash, with the addition of iron oxidizing bacteria. Results are similar to those results of a similar experiments in which ash from the same eruptions was dissolved in deionized water at varying acidity.

ACKNOWLEDGEMENTS

I would like to give thanks to Dr. Berry Lyons, Dr. Ellyn McFadden, Dr. Steve Goldsmith, Dr. Ian Howat, Dr. Jeff La Frenierre, and Dr. Bryan Mark for collecting ash samples. Dr. Carla Restrepo, Alma Quilo also collected samples from Pacaya with funding from NSF DEB 0919138. Dr. Steve Goldsmith's collection of Mt. Pinatubo's ash was made possible by NSF EAR HS 0443968. Without the work of sample collection this thesis would not be possible. I want to express my gratitude to Dr. Julie Sheets for allowing me to use the X-ray diffraction equipment and assisting me with the analysis of my samples. Thank you, Dr. Clara Chan, for providing bacteria cultures. NSF GEO EAR IF 1342632 allowed me to run my samples on the Dionex ion chromatographs. NSF GEO EAR IF 0744166 made using the Skalar SAN++ nutrient analyzer, which was critical to the project, possible. Shell Exploration and Production Company financially supported some of this research project. The Byrd Polar and Climate Research Center awarded me the McKenzie-Brecher Undergraduate Research Scholarship to fund my research. The School of Earth Sciences Field Experience Travel Fund helped fund my time at field camp.

Dr. Anne Carey, thank you for immediately scooping me up and into your amazing geoscience girl gang. Thank you for encouraging me to take extra math classes and for all the treats you've shared at meetings. Dr. Sue Welch, thank you for explaining complicated instrumentation with imaginative language, for helping me run my analyses, and for making wonderfully buttery cookies. I am incredibly grateful to both of my advisors for encouraging my growth as a scientist, while guiding me throughout my studies, research, and life as an undergraduate. I would not be where I am and who I am today without you.

Dr. Ashely Griffith, thank you for giving me the extra encouragement to continue being involved in geoscience outreach. Dr. Liz Griffith, thank you for helping me find fun experiments to share with kids.

Devin Smith, thank you for letting me squeeze into your car and your life. You've helped me find wonderful pals I couldn't do without. Also, the amount of work you put into anything and everything you do is ridiculously impressive. Becky Anderson, thank you for climbing rocks with me, sharing songs and support. Datu Adiatma, thank you for sharing your love of learning, geology, photography, and philosophy with me. Your excitement is contagious. Chris Conwell, thank you for being open and goofy. Also, thanks for taking me climbing (indoors and out). I admire your ability to put away snacks, crush rocks, and always find the energy to be incredibly kind to people. Teresa Avila, thank you for sharing the best books and smiles. Your thoughtfulness and creative abilities are unbelievably inspiring and sweet. Brittan Wogsland, thank you for sitting down with me at scheduled times every week to make sure we both actually write our theses. Thank you for screeching each time I enter a room, for always having snacks, and for hugs. Sam Carter, thank you for being so nice and coaxing iceman into my lap. Ji-Eun Kim, thank you for sharing fancy treats and for always being smiley. Thank you Casey Saup for sharing microgeobiology textbooks with me, for surreal cats, and for friendship. Thank you Sam Schneider and Danny Nyguen for making field work extra fun, for scrambling high and singing loud. A big thank you to all my geology pals for making The Ohio State University School of Earth Sciences feel like home. Having your support gave me the push I needed to write this thesis.

Mao, thank you for snuggling with me at night, for running to the door when I get home, and for making it impossible to sleep in.

I would also like to thank my parents for their love and support. Dad, thanks for wading through creeks with me and the pups, for teaching me the science of the best pies, biscuits, and cornbread. Mom, thank you for letting me roll around in the dirt, for always being prepared, for bringing me soup when I'm sick, for encouraging me to explore and for steering me towards geology. I love you both so much and couldn't have made it where I am or finished this thesis without you.

List of Figures

LIST OF TABLES

INTRODUCTION

The amount of CO_2 in the atmosphere over geologic timescales is greatly affected by the weathering of silicate and phosphate rocks (Berner *et al*., 1983; Berner, 1999). Weathering of Ca-Mg phases is significant because it results in precipitation of Ca Mg carbonates which affects long term CO_2 uptake. Weathering of iron or phosphate phases is important because these reactions release nutrients that promote plant growth and take up CO_2 as organic carbon in the short term (Karl et al., 1988). These processes regulate the CO_2 budget on long-term and short-term time scales, respectively. These weathering processes are potentially affected by surrounding life forms such as bacteria. Bioavailable iron is a key micronutrient for certain bacteria and it is important to study all the following processes to accurately define a global carbon budget.

GEOCHEMICAL BACKGROUND

Silicate weathering and its role as a carbon sink in geologic timescales

The weathering of calcium and magnesium rich silicates play an important role in the global carbon cycle. When silicate minerals such as plagioclase are weathered, they produce cations which react with carbon dioxide in water to form carbonate rock and sequester carbon dioxide.

Example Formula:

$$CaAl_2Si_2O_8 + 2CO_2 + 3H_2O \rightarrow Al_2Si_2O_5(OH)_4 + Ca^{2+} + 2HCO_3^-$$

(plagioclase + carbon dioxide +water → kaolinite + calcium ion+ carbonic acid)

$$Ca^{2+} + 2HCO_3^- \rightarrow CaCO_3 + CO_2 + H_2O$$

(calcium ion + carbonic acid → calcite + carbon dioxide +water)

As shown in the example equation above, when plagioclase is weathered there is a net loss of one mole carbon dioxide from the atmosphere via precipitation of calcite. Andesitic ashes are composed of a combination of glass and minerals. One of the most common minerals in andesitic igneous rocks is plagioclase. (Best and Christiansen, 2001)

There are many different factors that control the rates at which silicate minerals are weathered, this includes temperature, lithology, erosion rate and pH (Schopka et al., 2011, Kump and Brantley, 2020). Understanding the different controls on silicate weathering is important for understanding the global carbon cycle.

Iron and phosphorus as limiting species

The weathering of iron- and phosphorous-bearing minerals plays a role in the short term cycling of carbon dioxide. Iron and phosphorus are limiting nutrients for plants and phytoplankton. Therefore, the release of these nutrients by the weathering of volcanic ash can increase primary productivity in the ocean and on land (Karl et al., 1988). The release of these nutrients is dependent on multiple factors including pH (Kump and Brantley, 2020). Studying the controls on iron and phosphate dissolution from the weathering of volcanic ash is relevant to understanding the cycling of carbon dioxide on non-geologic time scales. When volcanic ashes fall in the ocean, the rate at which these nutrients are released is relevant for understanding what life will be able to access and use those nutrients.

Bacteria can mediate the release of nutrients. The growth of iron oxidizing bacteria like *Mariprofundus ferrooxydans* have been found in association with submarine volcanoes (Hodges and Olson, 2008). The presence of ferric iron adsorbed onto mineral surfaces can slow weathering rates and dramatically decrease the amount of iron and silica released from basaltic minerals such as fayalite (Santelli et al., 2001). The production of ferric iron by iron oxidizing bacteria (*Acidithiobacillus ferrooxidans*) decreased dissolution rates 50-98% (Santelli et al., 2001)

Dissolution of Volcanic minerals versus volcanic glass

Weathering rates are not only controlled by environmental factors such as pH and temperature, but also by the structural characteristics and composition of the feature being weathered, such as crystallinity, surface area, and chemical constitution (Kump and Brantley, 2000; White and Brantley, 1995). When comparing weathering rates for basaltic and felsic rocks, basalts are consistently weathered more rapidly than felsic rocks. The order of magnitude at which basalts weather faster than felsic rocks ranges from 10-100 times (Gudbrandsson et al., 2011).

Geologic setting

Samples were collected from five different stratovolcanoes around the world. Studying the dissolution kinetics of volcanic ashes is important because volcanic islands serve as major weathering hot spots. Despite only making up ~ 3% of the earth's surface, volcanic islands contribute ~ 30% of the global annual flux of particulate organic carbon to the ocean (lyons et al., 2002). Ash samples ranged in composition from basaltic andesite (Pacaya) to trachy dacite (Mt. Pinatubo). The SiO_2 weight percent of ash samples ranges from 51.59-62.24 (Table 1). Ash samples also vary in size and surface area.

Table 1. Ash Characterization Summary (Portier 2012)

	Tungurahua	**Pacaya**	**Eyjafjallajökull**	**Mount Pinatubo**	**Mount Saint Helens**
Classification	Andesite	Basaltic Andesite	Trachy-andesite	Trachy-dacite	Thrachy-andesite
Type of ash	fine	coarse	fine	coarse	fine
Specific surface area (ABET) (m2/g)	0.247	0.143	6.15	0.698	0.783
SiO_2	59.91	51.59	54.88	62.24	57.07
TiO_2	0.85	1.20	1.52	0.51	1.10
Al_2O_3	16.43	17.61	13.75	14.53	15.65
Fe_2O_3	10.97	11.1	9.72	4.47	6.65
MnO	0.11	0.18	0.22	0.11	0.10
MgO	4.43	4.97	2.34	2.35	2.6
CaO	6.73	8.79	5.02	4.59	5.93

Na_2O	3.83	3.39	9.50	7.86	8.27
K_2O	1.71	0.87	1.82	1.67	1.21
P_2O_5	0.23	0.26	0.36	0.19	0.23
Loss On Ignition	0.12	0.33	0.88	1.48	1.20
Total	101.32	99.96	99.12	98.52	98.8

Sample concentrations had precisions of ≤0.2 and accuracy of ±2%.

Mount Saint Helens

Mount Saint Helens is a stratovolcano located in Washington, USA. Mt. St. Helens has a maximum elevation of 8,363 feet and is built up by layers of andesite and basalt with a dome made of dacite (Cashman et al., 2005). In May of 1980 Mt. St. Helens erupted in an enormous pyroclastic flow. Ash particle size ranged from 63-4,000 micrometers. Previous studies of the ash mineralogy show that minerals found in the ash included plagioclase, hornblende, and pyroxenes (Fero et al., 2008; Farlow et al., 2012).

Mount Pinatubo

Mount Pinatubo exists in a chain of stratovolcanoes that are a part of the Bataan calc-alkaline arc at the southern end of the Luzon arc. Mt. Pinatubo has a hornblende-dacite dome built upon sedimentary rock, pyroclastic flow deposits, lahar, and an ultra-mafic complex (Pierson et al., 1992). June 12^{th} -15^{th} of 1991 Mt. Pinatubo erupted violently expelling ash, gas and lahars.

Pacaya

Pacaya is in Guatemala at the southern rim of Pleisticene Amatitlán caldera (Conway et al., 1992). Pacaya has frequent mild eruptions that produce cinders. It also has some occasional larger explosive eruptions. The eruption of May 2010 was comparatively mild, however, it still greatly impacted people living in Guatemala. For three different department locations, the Government of Guatemala declared a State of Calamity. The coarse ash covered water drainage systems and increased flooding risks. It also led to the temporary closure of the international airport in Guatemala (United Nations, 2010).

Tungurahua

The Tungurahua stratovolcano is in Ecuador at the eastern Andean cordillera and is one of the most active volcanoes in the area (Cruz-Reyna et al., 2010). Eruptions have varied in intensity. The eruption of interest for this study occurred in December of 2010. It was explosive and resulted in fine ash.

Eyjafjallajökull

The Eyjafjallajökull volcano is an ice-covered stratovolcano located in Iceland in the eastern volcanic zone. Iceland exists at the overlap of a spreading center and a hot spot. It is the only place on earth where mid ocean ridge is above sea level (Chapman, 2012).

Eyjafjallajökull has been volcanically active for some time. Before the 2010 eruption, the last dated eruption began December 19th of 1821 and subsided on January first of 1823 (Global Volcanism Program, 2013). In 1994 and 1999 scientists in Iceland observed intrusion events, however, no magma reached the surface during these events (NERC, 2018). There are also documented eruptions back to 920 BC (Keiding and Sigmarsson, 2011).

The 2010 eruption did not happen as one succinct event, instead occurring in phases over multiple days. At first, lava flowed from Eyjafjallajökull effusively. This fissure-fed phase allowed lava to reach maximum heights of about 100 meters, covering about 1.3 square kilometers with an average thickness of approximately 10-20 meters (NERC, 2018). This primary phase did not affect air traffic but it did impact local communities. The second phase of the eruption shut down air traffic for five days. Ejected ash particles reached heights of 8 km and about 140 million cubic meters of tephra were released in the first three days of this second phase eruption (NERC, 2018), which was not only more violent and impactful than the first, but also significantly faster. The rate of magma discharge second phase of the eruption was 10-20 times faster than that of the first phase (Thorardson et al., 2008).

The 2010 eruption of Eyjafjallajökull explosively expelled steam and pyroclastic fragments, including very fine ash. The size of ash expelled ranged from a few tens of nanometers greater than 300 μm in diameter. The ash contained andesitic glass, plagioclase, pyroxenes, and olivine (Gislason et al., 2010).

METHODS

Samples of ash from five different andesitic-dacitic stratovolcanoes were collected and analyzed for minerology using X-ray diffraction (XRD) and the PANanalytical HighScore Plus software. Dissolution rate experiments for silica and phosphate were conducted in synthetic sea water and a fresh water solution, with and without the addition of iron oxidizing bacteria. Data for silica and phosphate were obtained by running aliquots on the Skalar Sans++ nutrient analyzer. Experiments done in fresh water solution were analyzed for major cations on the Dionex DX 120 ion chromatograph equipped with AS40 automated sampler.

Ash Collection

Ashes were collected from five different eruptions in various parts of the world at an assortment of times post eruption. Information about sample collection and storage for each eruption is contained in table 2. Mount Saint Helens collection timing determined through personal communication with Dr. Berry Lyons.

Table 2. Ash Collection

	Eyjafjallajökull	Mount Saint Helens	Mount Pinatubo	Pacaya	Tungurahua
Eruption date	April-May 2010	March 1980	June 1991	May 2010	December 25, 2010
Collection timing	During the eruption	A short time after the eruption from an ash fall deposit	17 years after the eruption (2008)	6-7 hours after the eruption	During the eruption
Sample collector (s)	Dr. Ian Howat	Dr. Berry Lyons and Dr. Ellyn McFadden	Dr. Anne Carey and Dr. Steve Goldsmith	Alma Quilo	Jeff La Frenierre and Dr. Bryan Mark
Sample storage container	Nalgene bottle	Closed glass vial	Ziploc bag	Closed glass vial	Nalgene bottle

(Portier, 2012).

Ash Characterization

Bulk minerology of the ash samples was determined with powder X-ray diffraction (XRD) using a PANanylitical X-Pert Pro X-ray diffractometer. Each XRD scan measures the scattered X-ray intensities as a function of diffraction angle, 2-theta. The corresponding interplanar spacings (d-

spacings) of diffracting planes in the samples can be calculated from 2-theta and the wavelength of incident X-radiation. For the ash scans, CuKα radiation was used, and data were acquired over a 2-theta range of 5.01-69.99, with an X-ray tube voltage and current 45 keV, 40mA. Measured intensities and 2-theta values (and corresponding d-spacings) were analyzed using the PANanalytical HighScore Plus software and the International Centre for Diffraction Data (ICDD) PDF 4+ mineral reference database.

Solution Recipes

Seawater Solution (Modified from that of Dr. Sue Welch, personal comment)

0.42 M NaCl

0.01 M KCl

0.01 M $CaCl_2 \cdot H_2O$

0.05 M $MgCl_2 \cdot 6\ H_2O$

0.03 M $NaSO_4$

0.002 M $NaHCO_3$

Freshwater Solution (Dr. Sue Welch, Personal comment)

0.006 M $NaHCO_3$

Experimental Methods

Ash dissolution experiments were conducted in 0.5 L plastic Nalgene bottles. Each bottle was rinsed with deionized (18 MΩ) water and then soaked overnight with 18 MΩ water. The following morning the water was discarded and the 0.5 Liter Nalgene bottles were filled with 500 ml (±3 ml) of synthetic seawater solution. Then, one gram ±0.05 gram of ash was added to each bottle. A duplicate was made for each ash sample.

Samples were taken via syringe and filtered through 0.45 μm pore size 22 mm diameter disposable syringe filters. The syringe was rinsed with deionized water once and threaded once with unfiltered sample before sampling from a different bottle of ash solution. Before dispensing filter sample into a new sterile Falcon Max™ tube, about one ml of the sample was released into the sink to rinse the filter. The same filters were used for duplicates to conserve filters. After all samples were collected for a single time point, the syringe was rinsed three times with 18 MΩ water, taken apart, and left to air dry at room temperature in the lab. Samples (~10 ml) were taken from each bottle periodically over two years. At the start of the experiment samples were taken in intervals a few days. Later in the experiment samples were taken over longer intervals– weeks to months. Samples were analyzed on the Skalar SAN++ nutrient analyzer using methods provided by manufacturer.

SEM Sample Preparation

Small portions of ash samples (<0.5 g of ash) were transferred from the 0.5 L Nalgene bottles via disposable plastic pipettes onto a 0.4 micron Nucleopore filter attached to a manual vacuum pump. The sample was pumped and filtered. The same pipette used to transfer the sample onto the filter was then filled with 18 MΩ water and used to rinse the dry ash sample with deionized

water. The sample was pumped dry again and attached to a small metal post by use of double sided carbon tape. The same pipette was used for each sample collected but rinsed once with 18 MΩ water between sample collections. Samples were left out to air dry on the posts for a day on a lab counter. Samples were then coated with gold palladium and analyzed on the Scanning Electron Microscope at The Ohio State University a few days later.

IC Sample Preparation

Samples were poured into auto sampler vials up the marker (~5 mL). Filter caps were placed on unfiltered samples. Non-filter caps were placed on samples previously filtered with 0.4 μm pore size 22 mm diameter disposable filters. Samples and standards were then run on the Dionex DX 120 Ion Chromatograph equipped with AS40 Automated sampler at Ohio State University using the methods of Welch et. al. (2010).

Bacterial additions to experiments

Approximately 0.5 ml of growth medium containing *Marifundus ferrooxydans* was added to one set of the marine duplicates 259 days into the dissolution experiment. 0.5 ml of growth medium containing *Sideroxydans lithotrophicus* was added at the beginning of the freshwater dissolution experiments.

Freshwater microaerophilic lithotrophs (Clara Chan, personal communication)

Modified Wolfe's mineral medium (MWMM) per 1 L DI water

1 g NH_4Cl

0.2 g $MgSO_4 \cdot 7H_20$

0.1 g $CaCl_2 \cdot 2H_2O$

0.05 g K_2HPO_4

Saltwater microaerophilic lithotrophs (Clara Chan, personal communication):

Artificial saltwater (ASW) per 1 L DI water

27.5 g NaCl

5.38 g $MgCl_2 \cdot 6H_2O$

6.78 g $MgSO_4 \cdot 7H_2O$

0.72 g KCl

0.2 g $NaHCO_3$

1.4 g $CaCl_2 \cdot 2H_2O$

1.0 g NH_4Cl

0.05 g K_2HPO_4

RESULTS

Mineralogy

X-ray diffraction analysis for mineralogy identified some composition of plagioclase in each ash sample. Feldspars were identified in all samples and the feldspar compositions varied from more sodium rich to more calcium rich. Pyroxenes were identified in Tungurahua and Mount Saint Helens ash samples. Apatite, a phosphate mineral, was identified in ash from Mount Saint Helens, Mount Pinatubo, and Eyjafjallajökull. There were peaks in the spectra that were not attributed to minerals, so further analysis needs to be done.

Table. 3 Minerology of Ash Samples Determined by X-ray Diffraction

Phase	**Tungurahua**	**Mount Saint Helens**	**Mount Pinatubo**	**Eyjafjallajökull**	**Pacaya**
Feldspar	Albite $(Na_{1-y},Ca_y)Al_{2-3}Si_{3-2}O_8)$	Anorthite $(Ca_{1-y,}Na_{0-y})Al_{1-2}Si_{3-2}O_8$	Albite $(Na_{1-y},Ca_yAl_{2-3}Si_{3-2}O_8)$	Anorthoclase $(Na,K)AlSi_3O_8)$	Sodian anorthite $(Na_{1-y},Ca_yAl_{2-3}Si_{3-2}O_8)$
Pyroxene	Augite $(Ca,Na)(Mg,Fe,Al)(Si,Al)_2O_6$ Pigeonite$(Ca_xMg_yFe_z)(Mg_{y1}Fe_{z1})Si_2O_6$	Pigeonite $(Ca_xMg_yFe_z)(Mg_{y1}Fe_{z1})Si_2O_6$`			
Other phases		Apatite $Ca_5(Cl,OH)(PO_4)_3$ Quartz (SiO_2)	Fluoroapatite $Ca_5(PO_4)_3(OH,F,Cl)$ Anhydrite $(CaSO_4)$ Quartz (SiO_2)	strontium-apatite $(Sr,Ca)_5(PO_4)_3(F,OH)$	

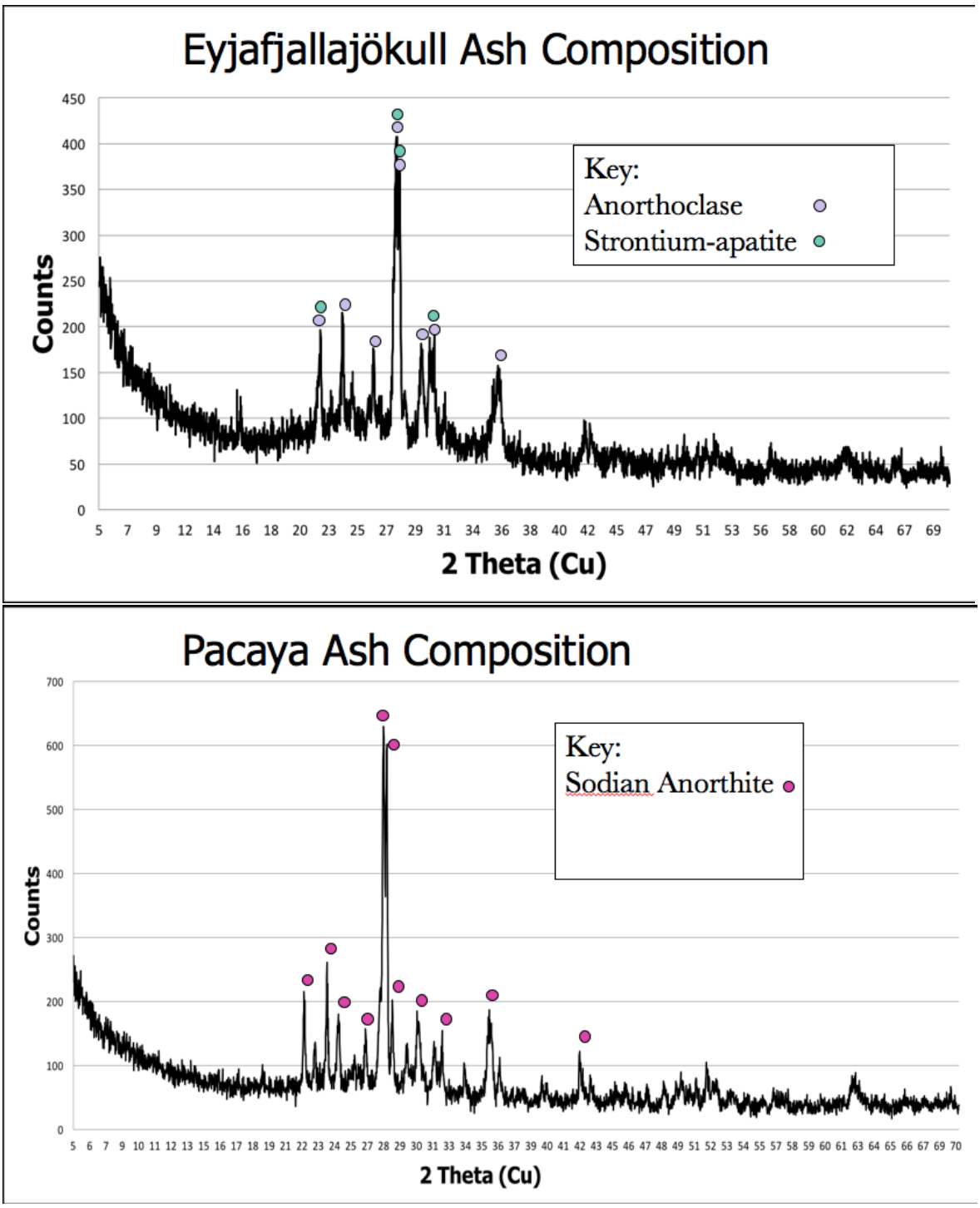

Figure 1. X-ray diffraction results of Pacaya and Eyjafjallajökull (Iceland) ash samples.

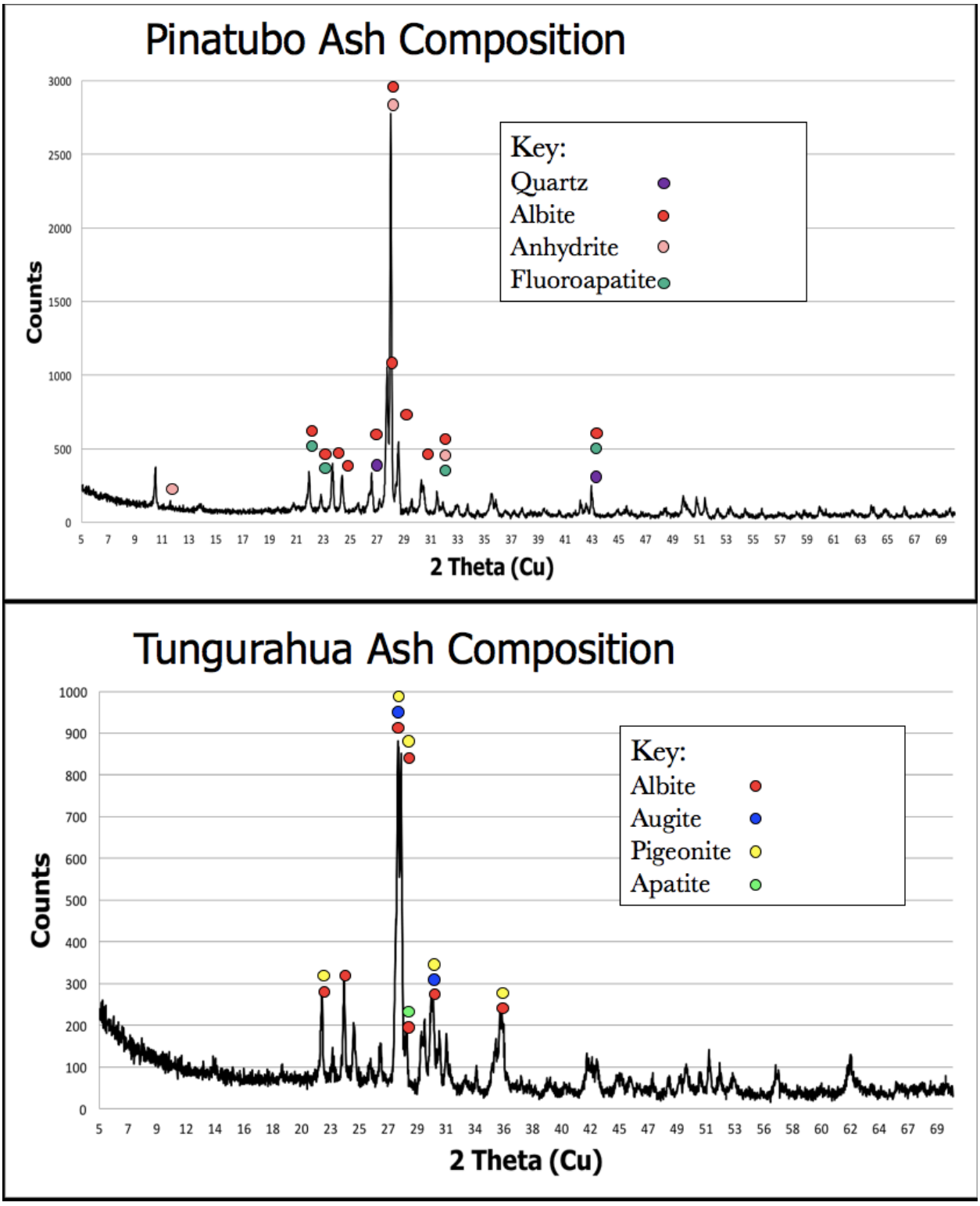

Figure 2. X-ray diffraction results of Tungurahua and Pinatubo ash samples.

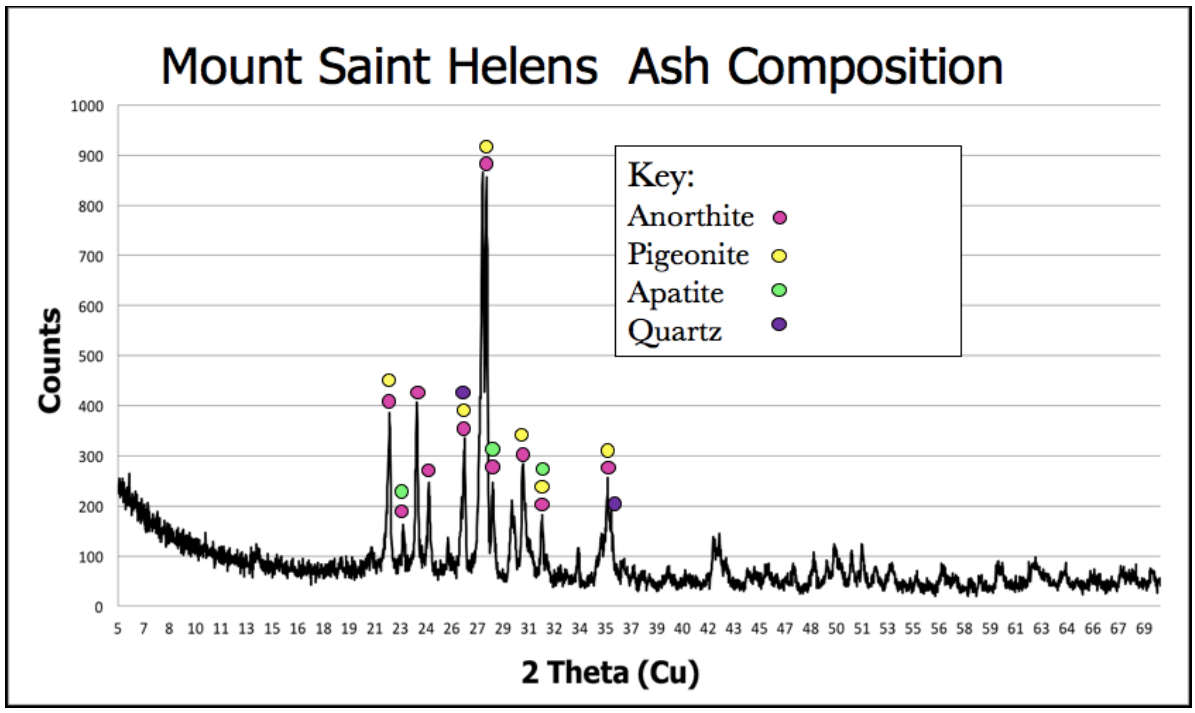

Figure 3. X-ray diffraction graphs for Mount Saint Helens ash samples (2-theta Cu vs counts).

Silica and phosphate release rates

The entire marine dissolution experiment spanned 834 days. *Mariprofundus ferrooxydans* were added to set 2 of marine dissolution experiments on day 260. Silica release rates over the course of the entire experiment were non-linear. However, release of Si was approximately linear when looking at three time segments of the experiment: initial, middle, and long term (Figure 4). Rates for marine experiments were calculated by linear fit in these three different time segments. The first 15 days yielded the highest release rates and were used to calculate the initial silica release rates. The next 245 days of the marine experiments were used to calculate the slower, middle rates. Long term marine Si dissolution rates solution were calculated from the over the final 574 days.

Fresh water experiments were conducted over 578 days, though because sampling frequency differed between these and the marine experiments, ash dissolution rates were calculated with a linear fit over two major time periods, initial and long term. The long term rates for fresh water experiments were calculated with only two time points. Release rates of silica were highest within the first 17 days and then slowed over next 561 days. Phosphate concentration measurements over the course of the experiments were frequently at or below the detection limit of the Sans Skalar++ nutrient analyzer and showed no systematic increase (Figure 5). The addition of iron oxidizing bacteria did not appear to affect the release of silica or phosphate.

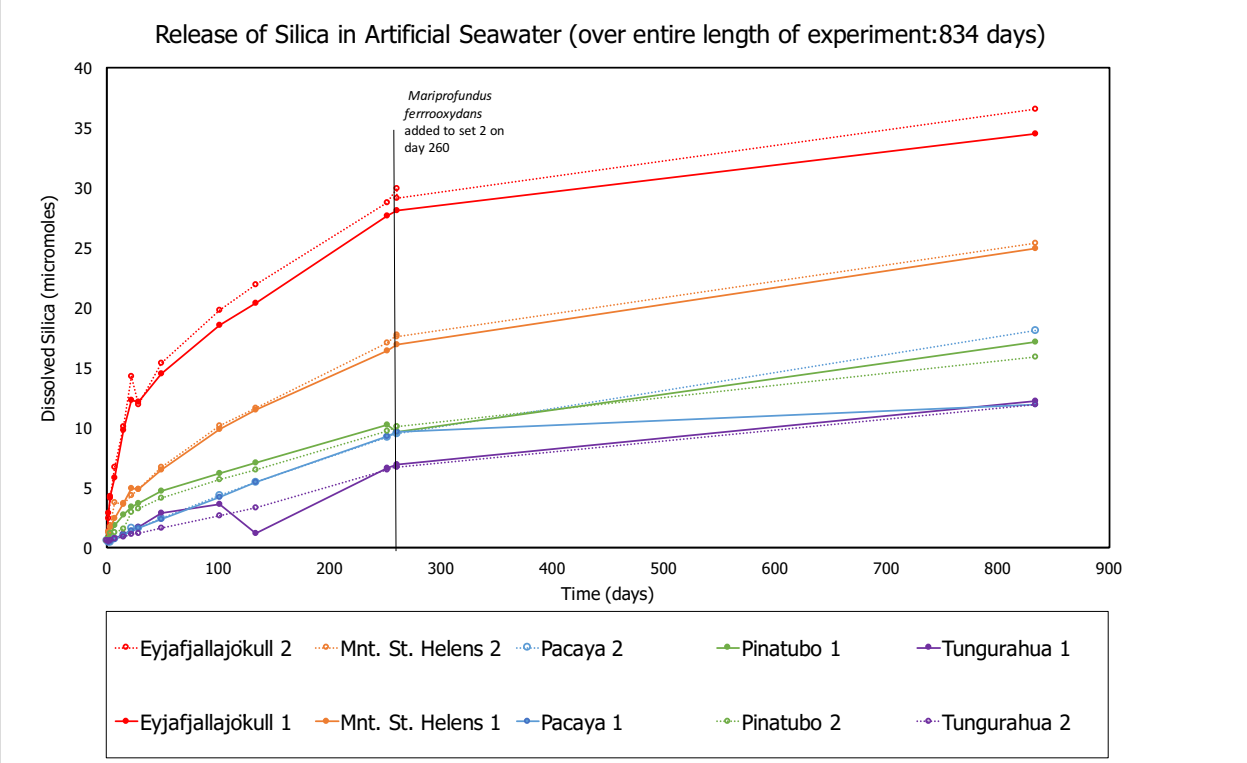
Release of Silica in Artificial Seawater (over entire length of experiment:834 days)
Mariprofundus ferrrooxydans added to set 2 on day 260
Dissolved Silica (micromoles)
Time (days)
0
5
10
15
20
25
30
35
40
0
100
200
300
400
500
600
700
800
900
Eyjafjallajökull 2
Mnt. St. Helens 2
Pacaya 2
Pinatubo 1
Tungurahua 1
Eyjafjallajökull 1
Mnt. St. Helens 1
Pacaya 1
Pinatubo 2
Tungurahua 2

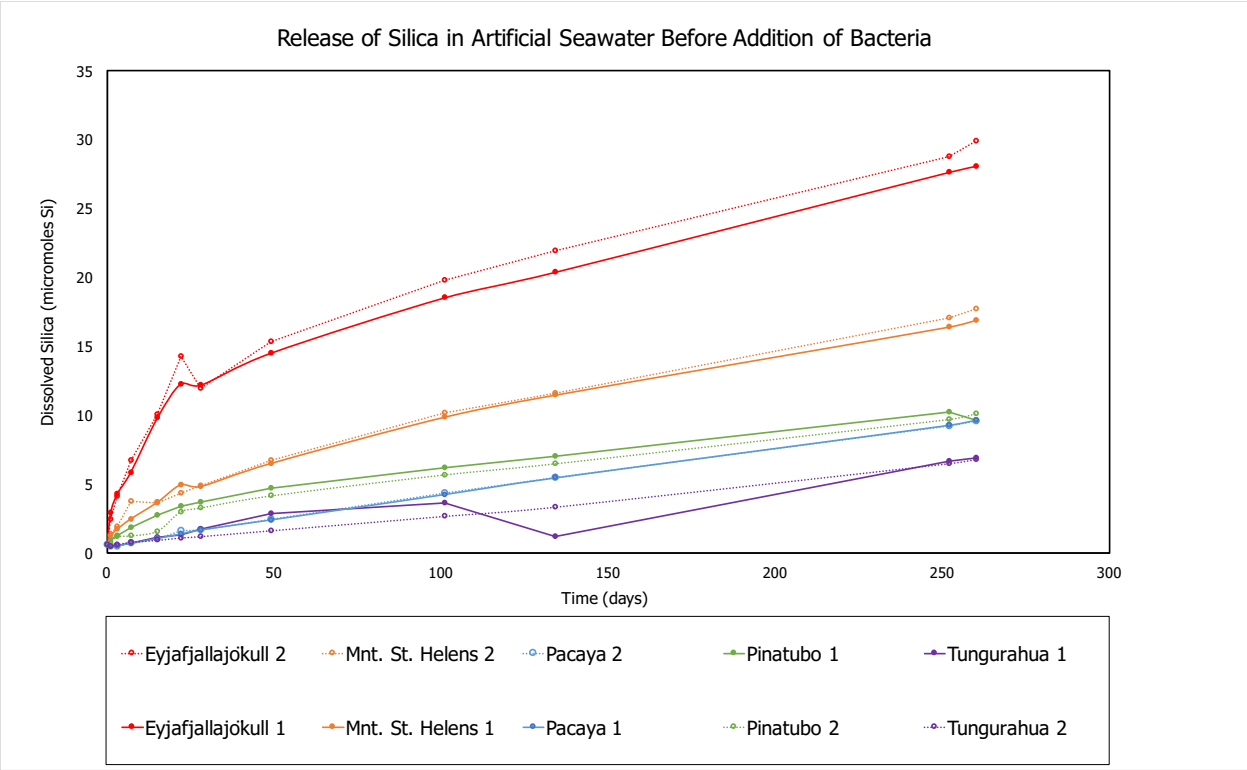
Release of Silica in Artificial Seawater Before Addition of Bacteria
Dissolved Silica (micromoles Si)
Time (days)
0
5
10
15
20
25
30
35
0
50
100
150
200
250
300
Eyjafjallajökull 2
Mnt. St. Helens 2
Pacaya 2
Pinatubo 1
Tungurahua 1
Eyjafjallajökull 1
Mnt. St. Helens 1
Pacaya 1
Pinatubo 2
Tungurahua 2

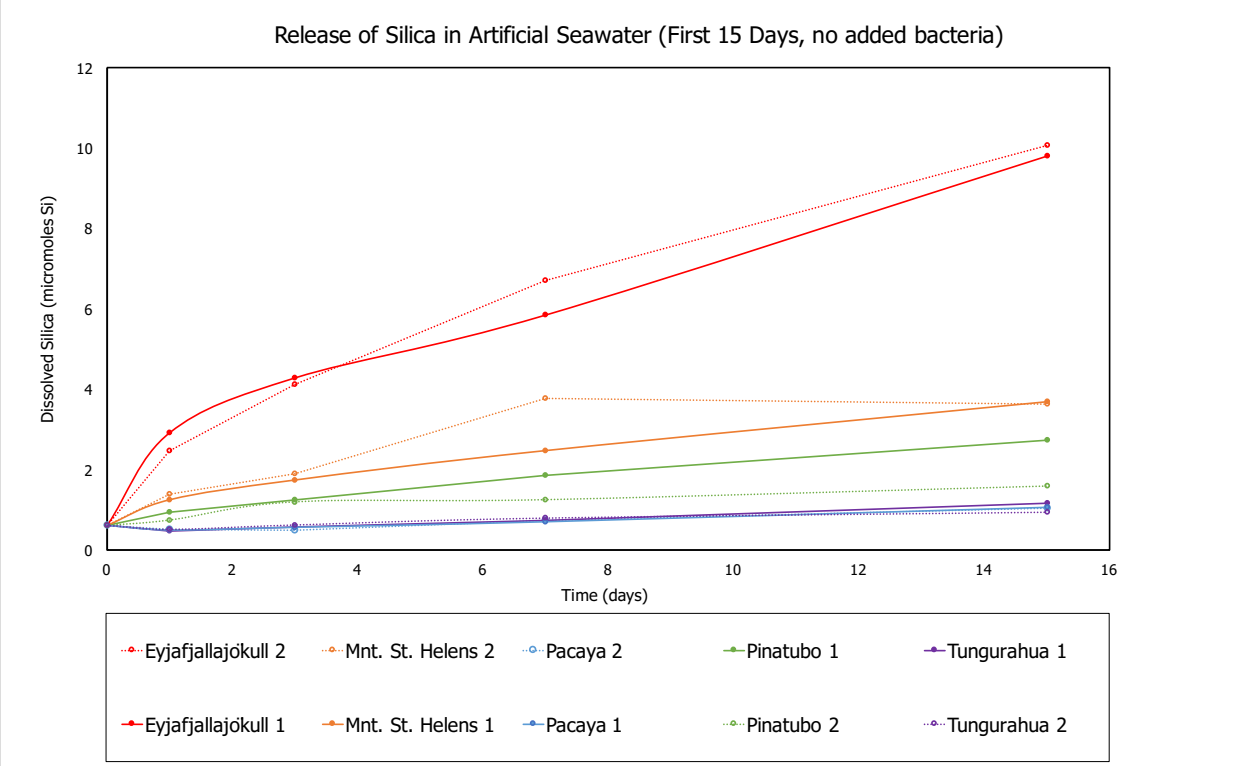

Figure 4. Marine Si release graphs: full length of experiment (834 days), before addition of *Mariprofundus ferrooxydans* (first 260 days), initial release (first 15 days).

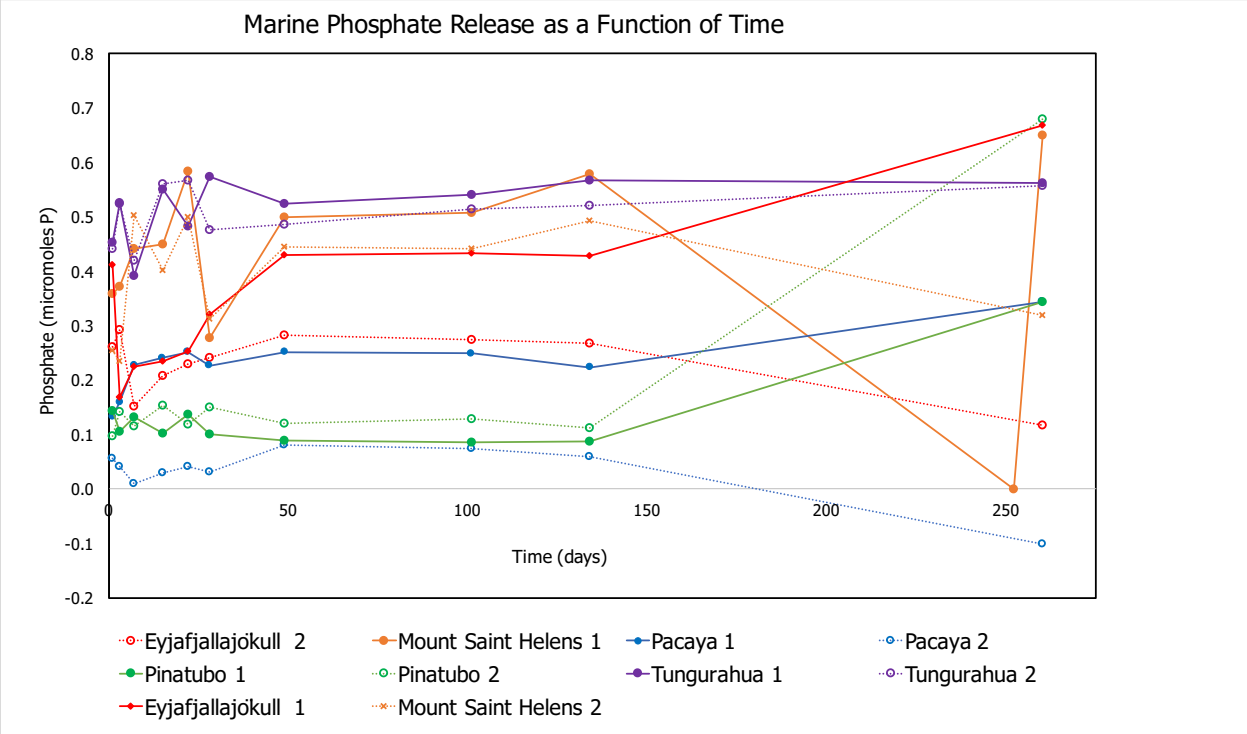

Figure 5. Marine phosphate release over time. (First 260 days, no addition of *Mariprofundus ferrooxydans*).

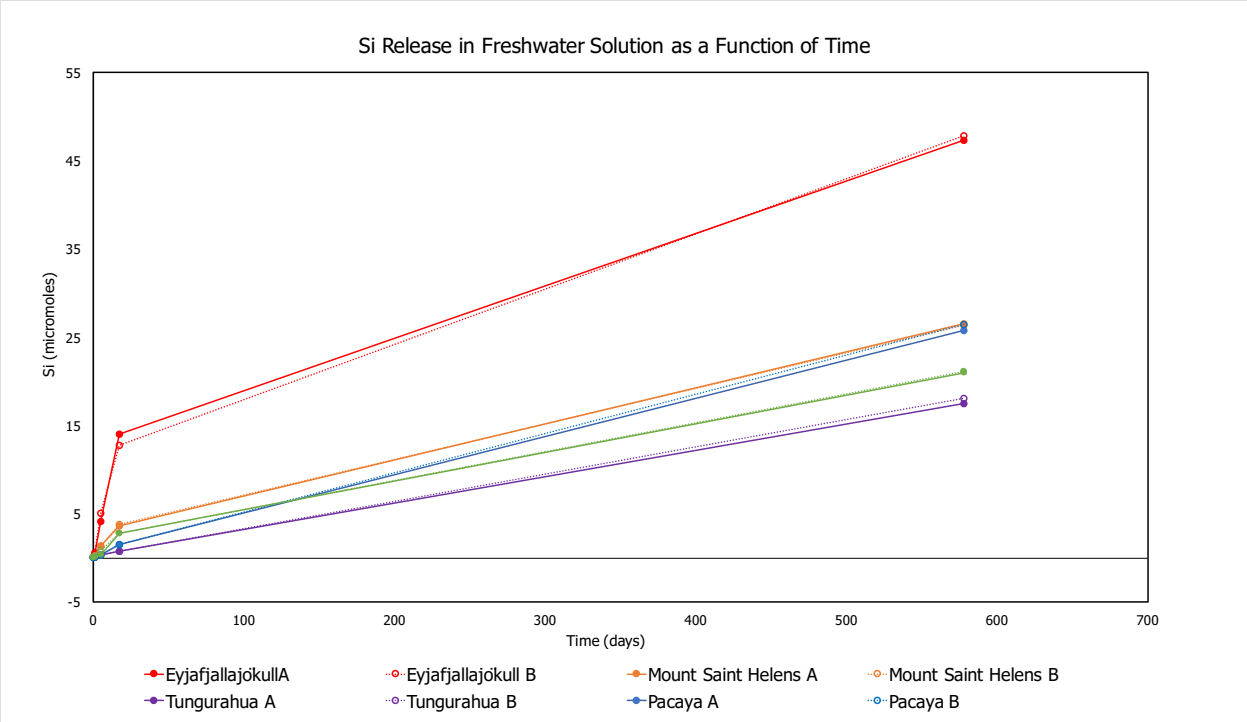
Si Release in Freshwater Solution as a Function of Time
Si (micromoles)
55
45
35
25
15
5
-5
0
100
200
300
400
500
600
700
Time (days)
EyjafjallajökullA
Eyjafjallajökull B
Mount Saint Helens A
Mount Saint Helens B
Tungurahua A
Tungurahua B
Pacaya A
Pacaya B

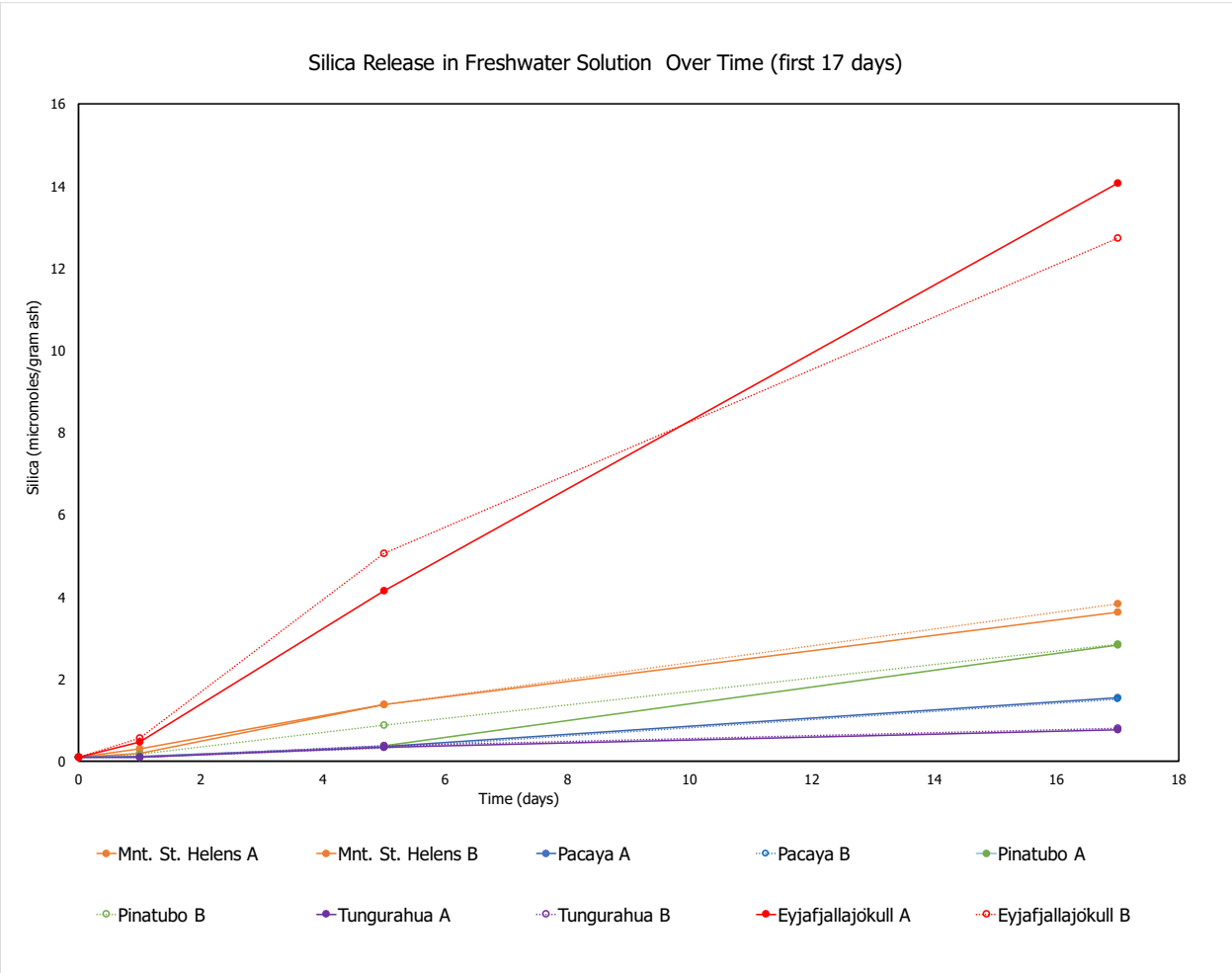
Silica Release in Freshwater Solution Over Time (first 17 days)
Silica (micromoles/gram ash)
16
14
12
10
8
6
4
2
0
0
2
4
6
8
10
12
14
16
18
Time (days)
Mnt. St. Helens A
Mnt. St. Helens B
Pacaya A
Pacaya B
Pinatubo A
Pinatubo B
Tungurahua A
Tungurahua B
Eyjafjallajökull A
Eyjafjallajökull B

Figure 6. Si release in freshwater solution over time: Full 578 days, First 17 days, A indicates no addition of bacteria, B indicates addition of *Sideroxydans lithotrophicus*

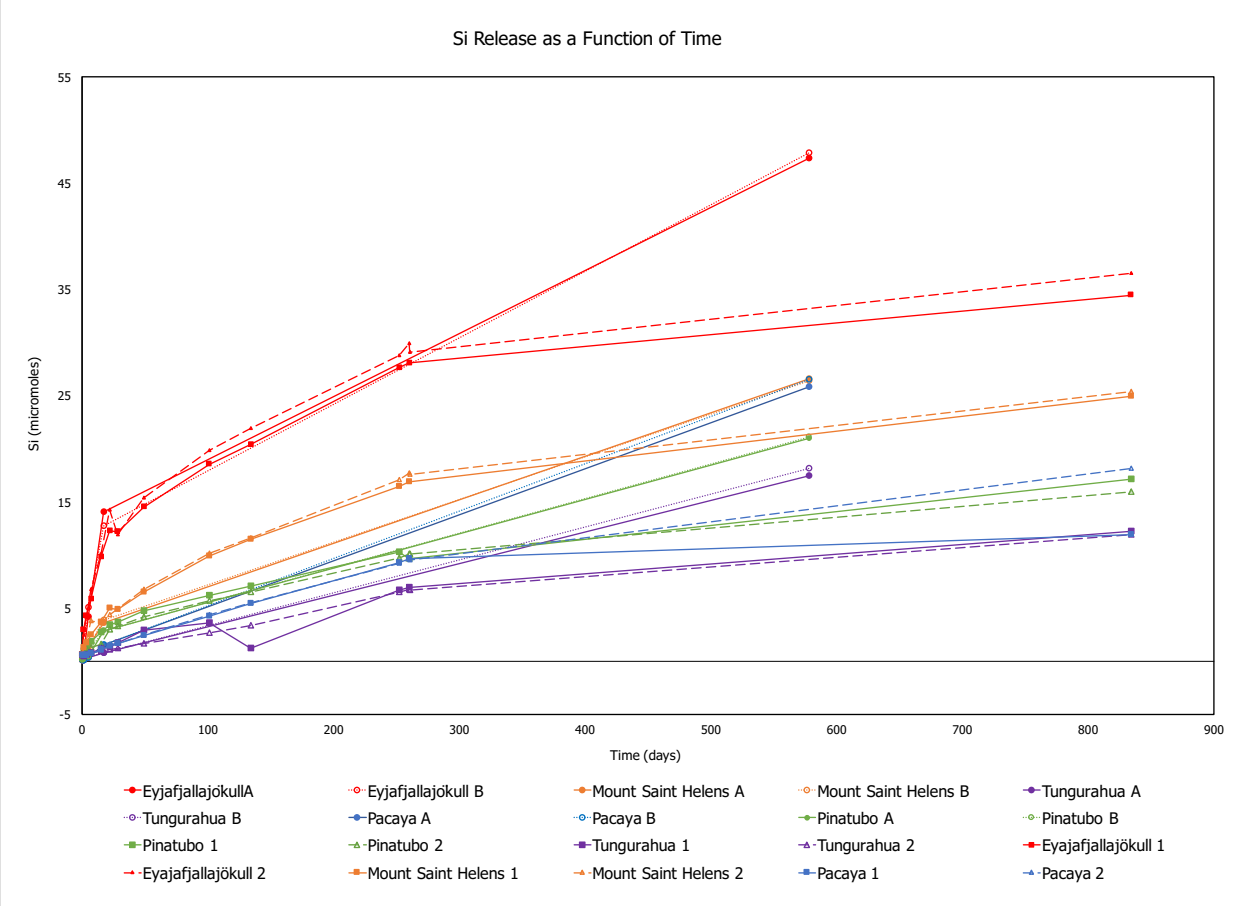

Figure 7. Si release over time for both marine and freshwater experiments (full length of experiments)

Si release rates in freshwater were similar or slightly faster than their marine counterparts until around 260 days into dissolution experiments. Around this time, the release rate of Si from many samples in marine solution began to decrease. Whereas, the Si release rate of samples in freshwater solution did not systematically slow down and dissolved Si concentrations of freshwater experiments surpassed those of all their marine counterparts (Figure 7).

Initial marine Si release rates of duplicates were comparable to each other. The difference between initial marine duplicate Si release rates ranged 0.00–0.68•10^{-6} µmole Si•m^{-2}•s^{-1}. Marine Si release rates of sets one and two remained similar after the addition of *Mariprofundus ferrooxydans* in growth media to set two.

Table 4. Comparing initial silica release rates (fresh vs. marine)

Ash Sample	Initial freshwater release rate (first 17 days) (μmole $Si \cdot m^{-2} \cdot s^{-1}$)	Ash Sample	Initial marine release rate (first 15 days) (μmole $Si \cdot m^{-2} \cdot s^{-1}$)
Eyjafjallajökull A	1.55E-06	Eyjafjallajökull 1	1.15E-06
Eyjafjallajökull B	1.40E-06	Eyjafjallajökull 2	1.19E-06
Mt. St. Helens A	3.06E-06	Mt. St. Helens 1	3.04E-06
Mt. St. Helens B	3.25E-06	Mt. St. Helens 2	2.58E-06
Pacaya A	6.90E-06	Pacaya 1	2.44E-06
Pacaya B	6.71E-06	Pacaya 2	2.34E-06
Pinatubo A	2.66E-06	Pinatubo 1	2.35E-06
Pinatubo B	2.67E-06	Pinatubo 2	2.35E-06
Tungurahua A	1.83E-06	Tungurahua 1	1.71E-06
Tungurahua B	1.91E-06	Tungurahua 2	1.03E-06

*A indicates no addition of bacteria

**B indicates the addition of *Sideroxydans lithotrophicus*

Silica dissolution rates were converted to units of μmole $Si \cdot m^{-2} \cdot s^{-1}$ to normalize rates for specific surface area of ash and for comparison to previous rate studies. Ash from Eyjafjallajökull on average, had the slowest initial release rate of silica in fresh and marine experiments, when normalized to surface area (Table 4). Pacaya had the fastest initial silica release rate of the freshwater experiments. There was no systematic difference between freshwater experiments done with or without the addition of *Sideroxydans lithotrophicus.*

Table 5. Comparing long term silica release rates

Ash Sample	Final Freshwater release rate (from day 17 to 578) (μmole $Si \cdot m^{-2} \cdot s^{-1}$)	Ash Sample	Middle Marine release rate (from day 15 to day 260 before addition of bacteria) (μmole $Si \cdot m^{-2} \cdot s^{-1}$)	Final marine Si release rate (*Mariprofundus ferrooxydans* added to set 2 on day 260.5) (day 260 to 834) (μmole $Si \cdot m^{-2} \cdot s^{-1}$)
Eyjafjallajökull A	1.12E-07	Eyjafjallajökull 1	1.40E-07	2.09E-08
Eyjafjallajökull B	1.18E-07	Eyjafjallajökull 2	1.52E-07	2.16E-08
Mt. St. Helens A	6.04E-07	Mt. St. Helens 1	7.97E-07	2.07E-07
Mt. St. Helens B	5.94E-07	Mt. St. Helens 2	8.49E-07	1.98E-07
Pacaya A	3.50E-06	Pacaya 1	2.83E-06	3.22E-07
Pacaya B	3.60E-06	Pacaya 2	2.83E-06	1.20E-06
Pinatubo A	5.36E-07	Pinatubo 1	4.67E-07	2.16E-07
Pinatubo B	5.40E-07	Pinatubo 2	5.77E-07	1.68E-07
Tungurahua A	1.39E-06	Tungurahua 1	1.10E-06	4.35E-07
Tungurahua B	1.447E-06	Tungurahua 2	1.11E-06	4.21E-07

Table 6. Comparing initial, middle, and final marine Si release

Sample	Initial marine Si release rate (first 15 days) (μmole Si•m^{-2}•s^{-1})	Middle marine Si release rate (from day 15 to day 260 before addition of bacteria) (μmole Si•m^{-2}•s^{-1})	Final marine Si release rate (*Mariprofundus ferrooxydans* added to set 2 on day 260.5) (day 260 to 834) (μmole Si•m^{-2}•s^{-1})
Eyjafjallajökull 1	1.15E-06	1.40E-07	2.09E-08
Eyjafjallajökull 2	1.19E-06	1.52E-07	2.16E-08
Mt. St. Helens 1	3.04E-06	7.97E-07	2.07E-07
Mt. St. Helens 2	2.58E-06	8.49E-07	1.98E-07
Pacaya 1	2.44E-06	2.83E-06	3.22E-07
Pacaya 2	2.34E-06	2.83E-06	1.20E-06
Pinatubo 1	2.35E-06	4.67E-07	2.16E-07
Pinatubo 2	2.35E-06	5.77E-07	1.68E-07
Tungurahua 1	1.71E-06	1.10E-06	4.35E-07
Tungurahua 2	1.03E-06	1.11E-06	4.21E-07

Marine release rates of Si on average were fastest the first 15 days of dissolution experiments and slowed over time.

Cation data

Concentration of dissolved major cations were measured for fresh water experiments on the ion chromatograph at three time points spanning 530 days. Cations measured include calcium, potassium, lithium, sodium, and magnesium. Overall, sodium was the most abundant cation in every sample. This was not corrected for the amount of sodium present in the freshwater solution recipe. The next most abundant cation was calcium. Detectable cation concentrations increased within the first two weeks of dissolution and then remained approximately stable over time. Most measurements for lithium were below the detection limit for the instrument. Potassium concentrations were below detection for many samples. Eyjafjallajökull ash samples had some

detectable concentrations measured that indicated no change in concentration of potassium over 530 days.

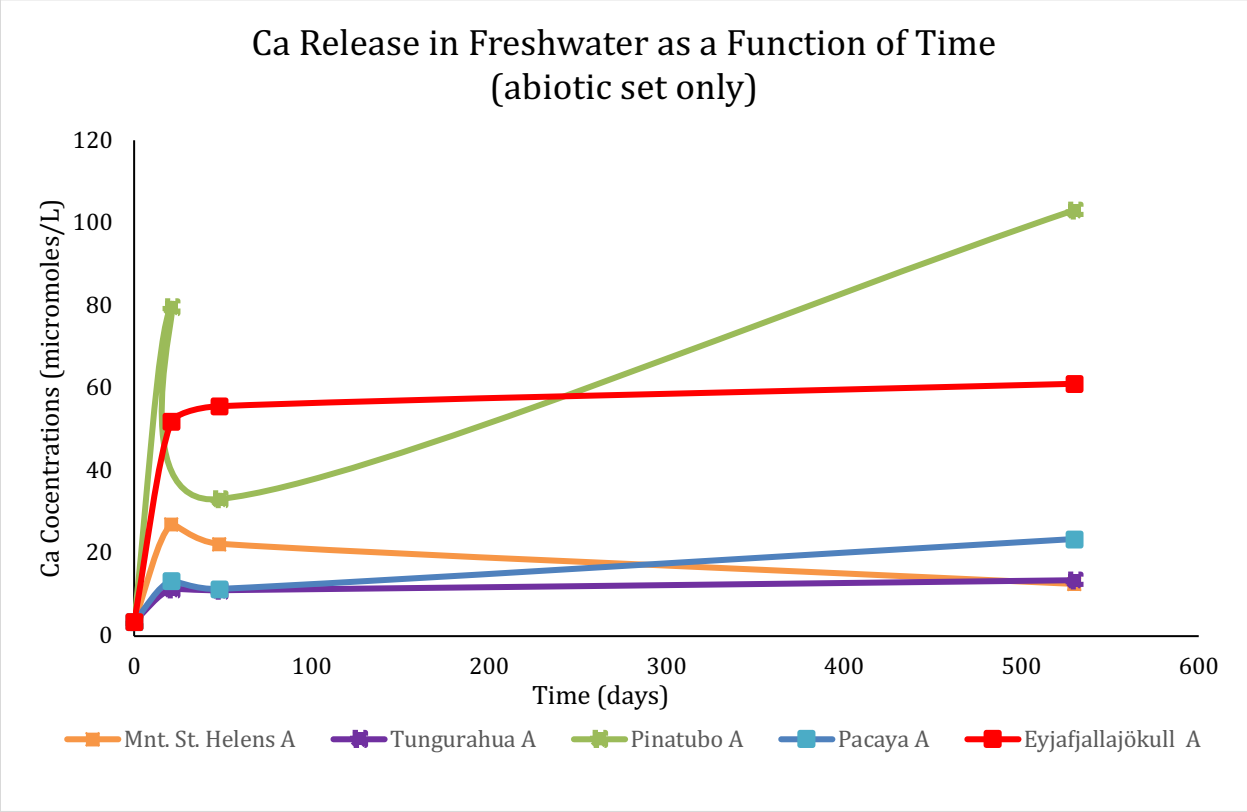

Figure 8. Calcium concentrations in freshwater samples of set A (the set without added bacteria).

Scanning electron microscope results

Pictures of ash samples were taken at the conclusion of dissolution experiments on the scanning electron microscope (SEM). Dissolution etch pits were not observed on any of the samples, mineral surfaces had sharp edges and there were abundant fine particles throughout the samples. Pictures were selected to display general ash minerology and texture as well as compelling features.

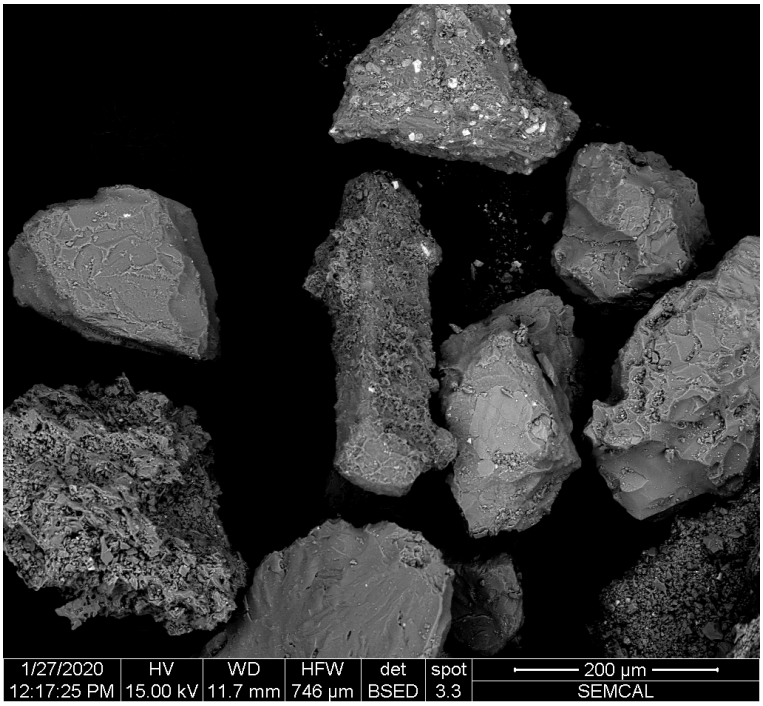

Figure 9. SEM image of Mount Saint Helens ash sample at conclusion of marine dissolution experiments.

Mount Saint Helens ash samples contained a combination of glassy and crystalline materials. This is clearly shown by the variety of shapes and textures displayed in fFgure 9. The SEM image of Mt. St. Helens ash (Figure 9) shows a crystalline structure in the center of the page. It is composed of silica, oxygen, aluminum, and sodium. This along with the shape, suggest that it could be sodium rich plagioclase. The mineral in the center is situated between lighter colored glassy structures. The difference in grayscale indicates that the glass contains heavier elements than the mineral. At the top of the image there is a gray glassy body with lighter crystalline structures on its surface. The lighter minerals are iron rich.

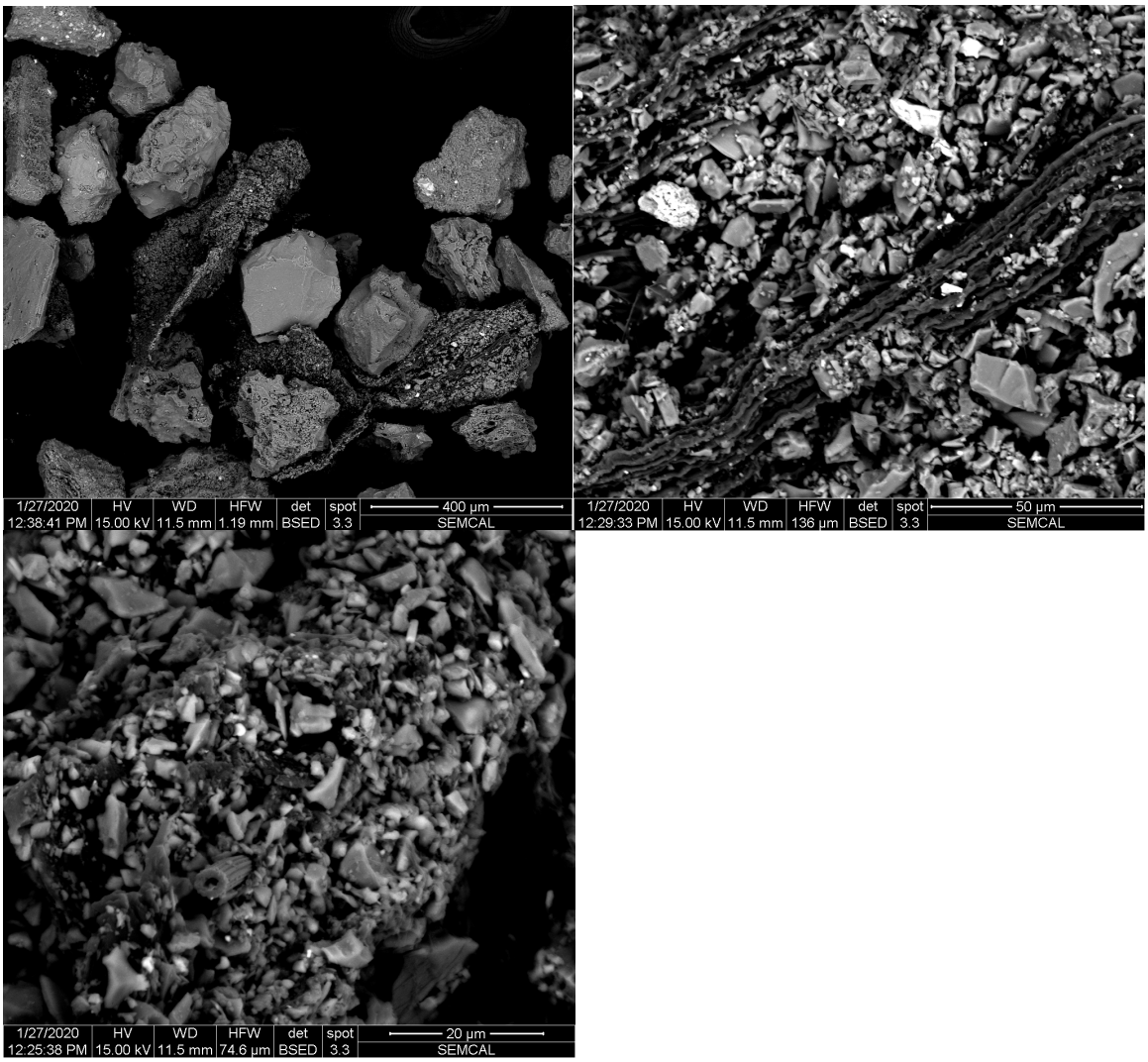

Figure 10. Mt. St. Helens ash sample post marine dissolution experiments: top left 10.a, top right 10.b: Organic material as seen in bottom left of 10.a.. Bottom left image: Mt. St. Helens ash sample post marine dissolution experiments: tube structure.

The most evidence of organic material was observed on the Mt. St. Helens ash samples. The extent of organic material present is displayed in SEM image of the ash (Figure 10). The large dark feature in the bottom left of image, engulfing the lighter gray material, is composed mainly of carbon. The dark gray undulating organic material is shown in more detail in Figure 10.b. The dark organic material is covered with small fragments of glass. The lighter fragments are likely iron-rich based on the measured chemical composition of larger visually similar structures found in the Mt. St. Helens ash sample. Tube shaped structures were observed surrounded by organic material encrusted in ash fragments (Figure 10).

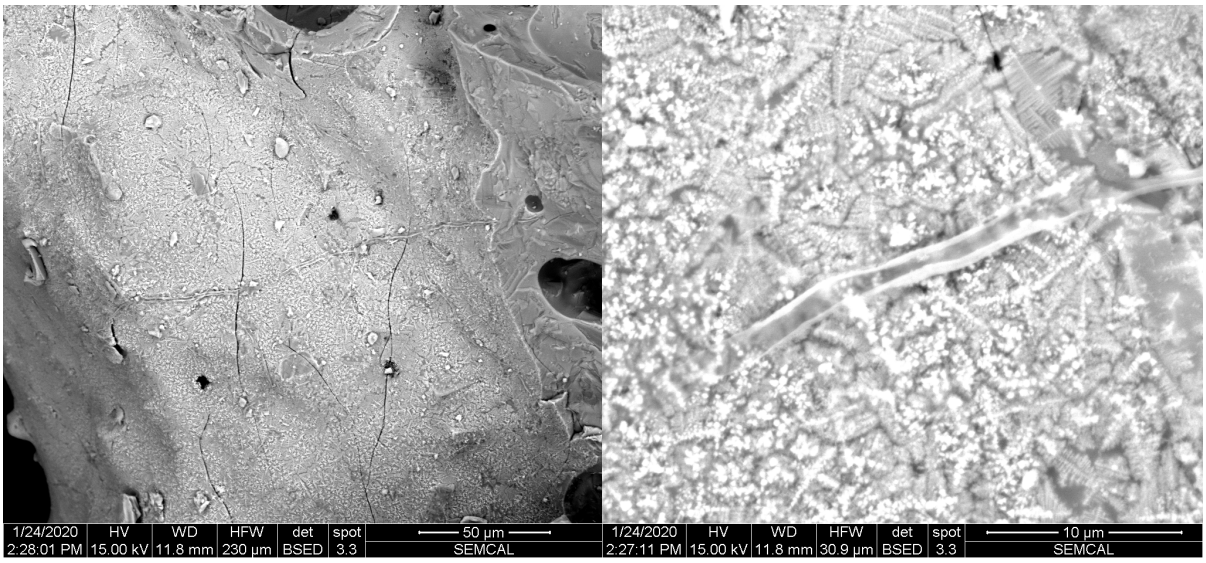

Figure 11. Left: figure 11.a: Pacaya Ash samples at conclusion of freshwater dissolution experiment. Right: figure 11.b, close image of tube structure seen in 11.a

Light colored features, largely composed of Ti, Fe and oxygen, were observed on the surface of Pacaya ash samples (Figures 11.a and 11.b). These iron hydroxides have a feathery texture and appear on the surface of a glassy specimen, suggesting they may be the result of devitrification. The surface of the glassy specimen also displays small fractures and vesicles (Figure 11a). Tube structures similar to those observed in Mt. St. Helens ash samples were also observed scarcely on Pacaya ash samples. The tube structures can be seen cutting across the middle of the specimen (Figure 11a). The tube structure has been altered (Figure 11b); it is not a complete tube like the tube viewed on Mt. St. Helens ash. It seems to have burst or been eroded. The tube was too small and thin to get a proper measurement of chemical composition. However, based on the light color, it likely contains iron.

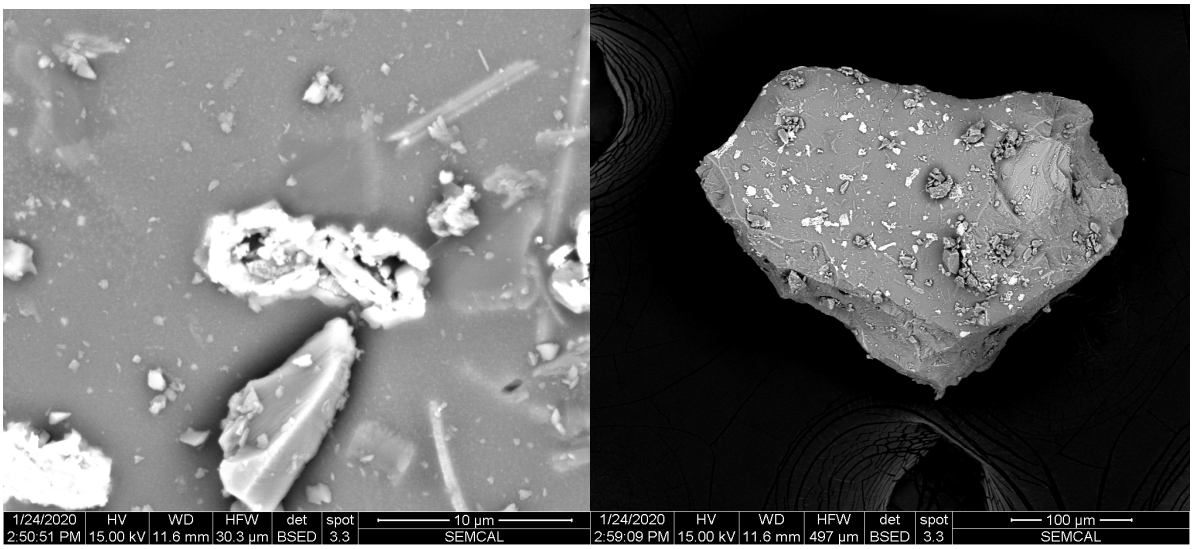

Figure 12. Right: 12a: Tungurahua ash after freshwater dissolution experiments. Left: 12b close view of light colored altered mineral on surface of ash Tungurahua ash particle.

Tungurahua ash consists mainly of medium to dark gray glassy material with small light colored crystalline features (Figure 1.a). The SEM image from Tungurahua (Figure 12b) shows a light-colored mineral in the center, which is highly altered with iron oxides forming on surface. The shape along with knowledge of minerology from X-ray diffraction suggests that the altered mineral may have been a pyroxene. It is surrounded by darker, less iron rich, glassy material.

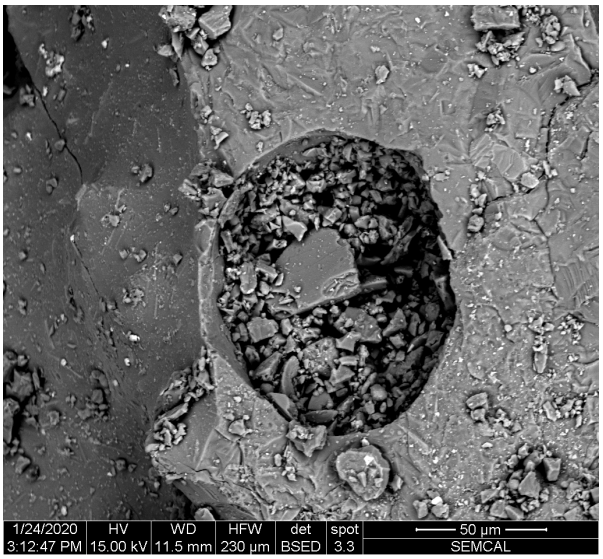

Figure 13. Tungurahua ash post freshwater dissolution experiments

The SEM image of Tungurahua ash (Figure 13) shows pits on the surface of glass fragments full of smaller glassy material. This displays the rougher texture present in small concentrated areas of Tungurahua ash.

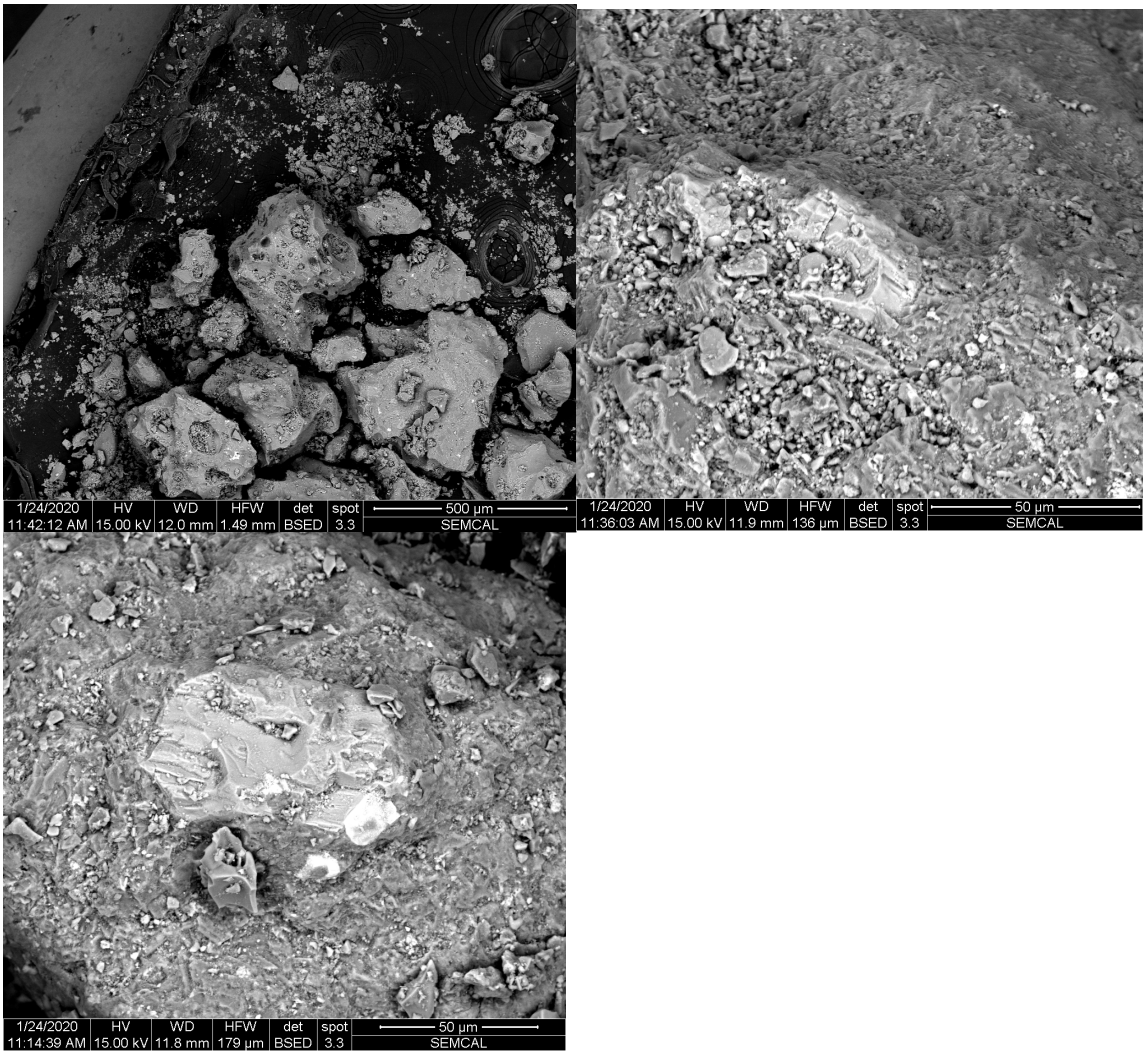

Figure 14: Eyjafjallajökull ash after freshwater dissolution experiments

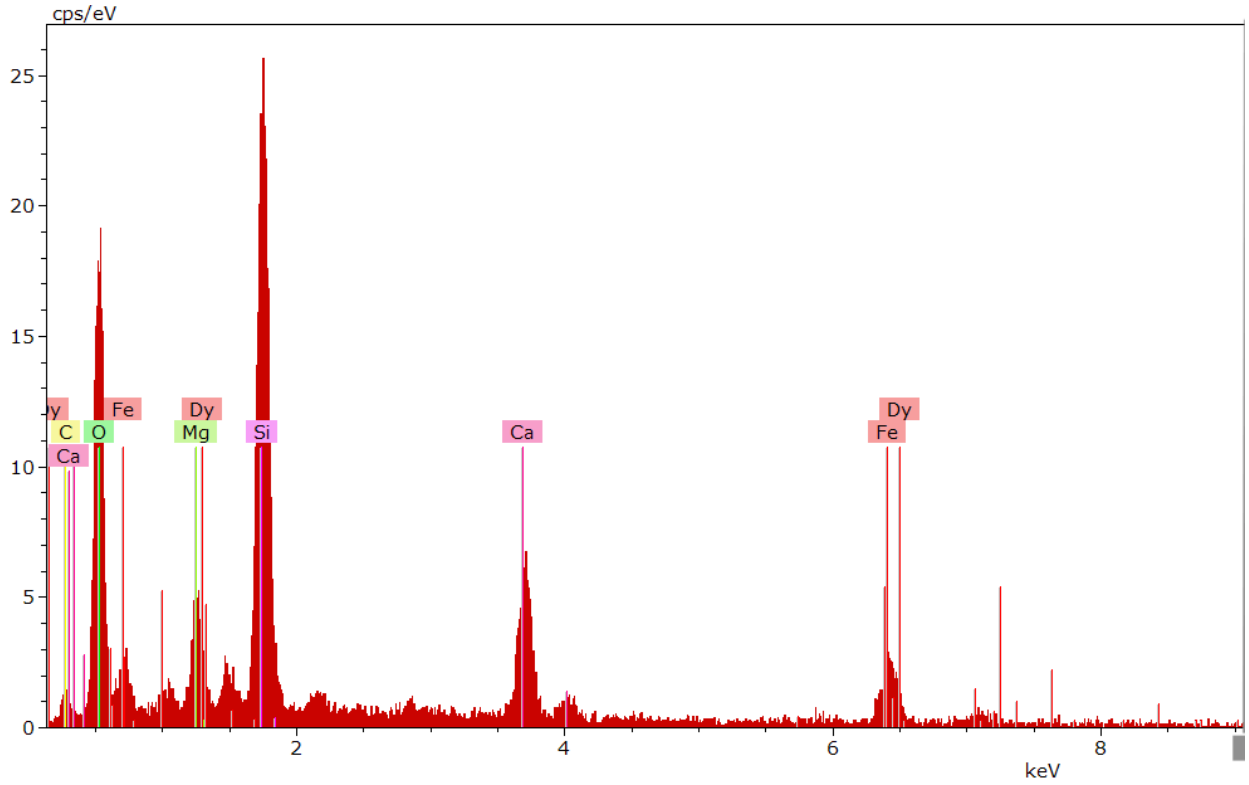

Figure 15. Detector energy dispersive x-ray spectrometer (EDX) reading of mineral in Eyjafjallajökull ash displayed in bottom left image of Figure 14

Eyjafjallajökull ash had the highest specific surface area of all the ash samples. The Eyjafjallajökull ash has many very fine fragments and a rough surface (Figure 14). Most of the ash is a medium gray andesitic glass. The lighter euhedral mineral (bottom left image of Figure 14) was composed of silica, oxygen, iron, magnesium and calcium which suggests that it is likely augite. Augite was not detected on XRD analysis. It is surrounded by rough andesitic glass.

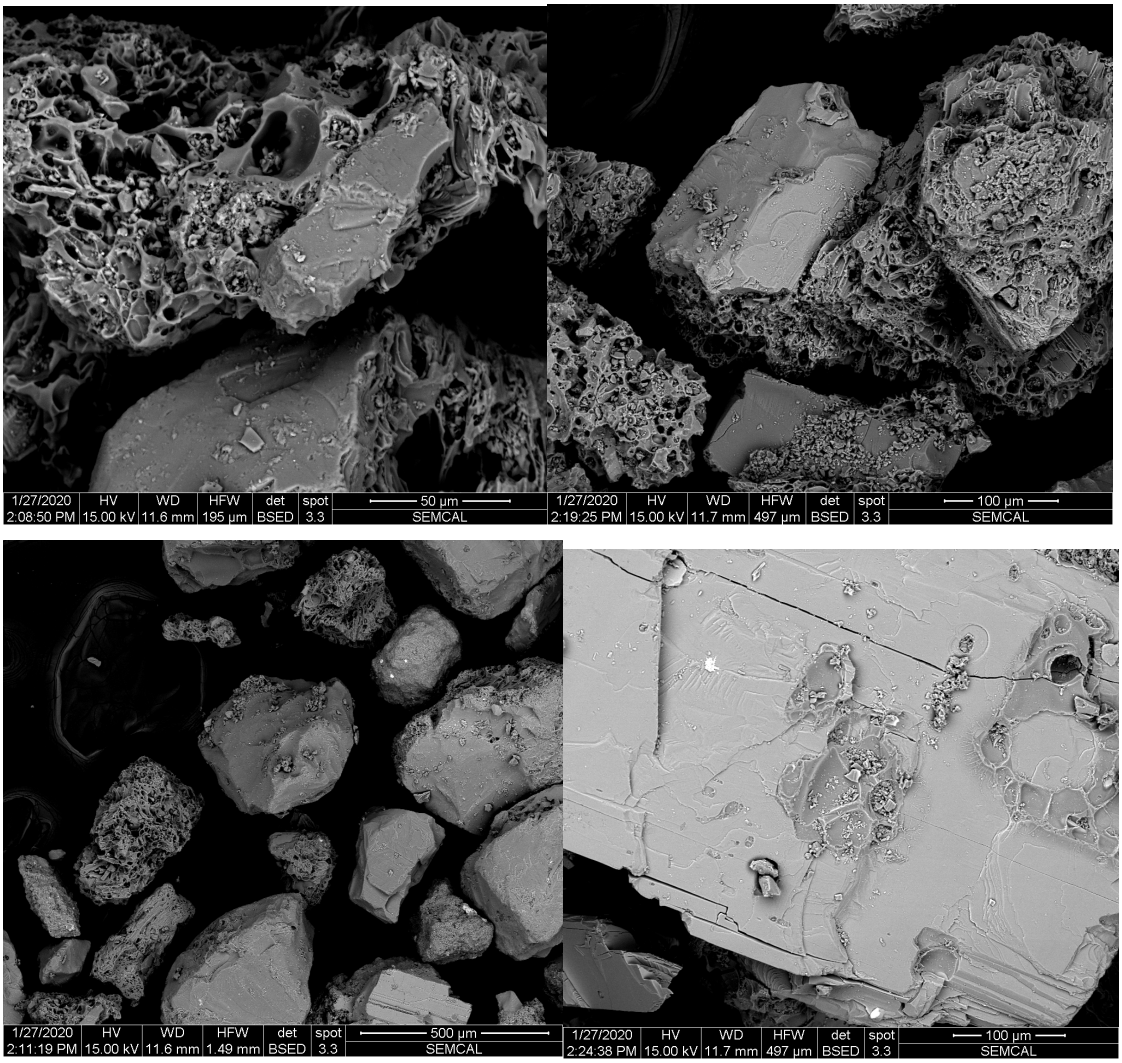

Figure 16. Pinatubo ash after freshwater dissolution experiments. 16a (top left), 16b (top right), 16c (bottom left), 16d (bottom right).

Pinatubo ash samples consist of glassy and crystalline structures (Figure 16). Some large light colored minerals had glassy features on the surface that look like ruptured bubbles (Figure 16d). Within these features small crystalline structures were observed that consisted of mainly calcium and phosphorous, indicating that they are likely small apatite crystals. Pinatubo ash samples display a range of textures. Many glasses are highly vesicular (Figures 16a, 16b, 16c), while crystalline structures are smooth. Crystalline structures rage from euhedral to anhedral.

Discussion

Silica Dissolution

Dissolution rates observed of andesitic ashes in fresh water solution and marine solution can be compared to similar experiments done conducted at circumneutral pH. Initial silica release rates normalized for specific surface area were slowest for Eyjafjallajökull , in marine and freshwater experiments. In previous experiments preformed at neutral pH, with samples from the same five eruptions, Eyjafjallajökull also had the slowest silica release rate (Portier, 2012). However, in the same work, Tungurahua was found to have a faster silica release rate than Pacaya by approximately 0.3 ($\log(\mu mol\ Si \bullet m^{-2} \bullet s^{-1})$), whereas in this study, Pacaya was found to have a faster release rate of silica in fresh and marine solutions. Pacaya ash is compositionally the least felsic of the five different eruptions (51.59 wt %).

Pacaya ash also had the smallest specific surface of 0.143 m^2/g, among the ash samples tested(Portier 2012). Since the measured specific surface area of Pacaya ash was so small, normalizing release rates for surface area had little impact on the dissolution rates. Ash from Eyjafjallajökull had the highest measured specific surface area before dissolution experiments (6.15 m^2/g). This means that normalizing release rates for specific surface area lowered them much more for Eyjafjallajökull compared to Pacaya and Tungurahua. Surface area is an important variable when it comes to weathering rates, however, not all surface area is equally reactive. Other work has suggested that geometric specific surface area of glasses is more proportional to their dissolution rate than BET specific surface area (Wolff-Boenisch et al., 2004). BET surface area can account for potentially unreactive internal micropores (Anbeek 1992, 1993).

In general, release of silica was equivalent or slightly faster in freshwater solution compared to marine solution. This is somewhat unexpected. Previous work found that amorphous silica dissolves much faster in the presence of salts (Dove et al., 2008). However, the freshwater experiments were not done in pure deionized 18 MΩ water. They were performed in a dilute sodium bicarbonate solution. Statistical analysis was not done on the significance of the freshwater rates compared to the marine release rates.

Silica release can also be compared to glass dissolution experiments done in basic and acidic conditions. Based on a previous study of dissolution of andesitic ashes, silica release increased by orders of magnitude with decreasing pH (Portier, 2012). Near neutral pH dissolution rates of crystalline basalt from other studies ranged ~2–10 times faster than initial marine rates determined in this study (Gudbrandsson et al., 2011). Rates determined from basaltic glass ranged from $1.38*10^{-15}$(mol $Si/cm^2/s$) to $4.17*10^{-15}$(mol $Si/cm^2/s$) (Gislason and Oelkers, 2003).

Phosphate Release

Phosphate release was not as consistent as silica release. Rates estimated using a linear fit were approximately 0 μmol P/gram ash/day for all experiments. This is consistent with phosphorous release rates conducted at pH 4 for glasses over range of compositions, mafic to felsic (Wolff-Boenisch, 2004). Unaltered apatite crystals were identified via SEM on Pinatubo ash. Apatite is a key potential source of dissolved phosphate. Dissolution experiments preformed in acidic

solution with ashes from Mount Saint Helens and Mount Pinatubo resulted in the dissolution of apatite crystals (Portier, 2012).

Dissolution of apatite would be the primary mineralogical source of phosphate from Pinatubo, Eyjafjallajökull, and Mount Saint Helens ashes. No hexagonal dissolution pits were found via SEM imaging at the conclusion of dissolution experiments. Crystals of not visibly altered apatite were found on the surface Pinatubo ashes. The apatite in Mount Pinatubo ash was determined by XRD analysis to contain Fluorine. Fluorine bearing apatite is less soluble than non-fluorine bearing apatite (Rey, 2008). Anhydrite was identified only in ash from Mount Pinatubo. Quartz was identified in Mount Saint Helens and Mount Pinatubo ash.

Minerology

Based on XRD plagioclase was confirmed to be present in all samples and appeared to be the most abundant mineral phase based on the peak intensities in the XRD spectra. SEM analysis also indicated the presence of crystalline structures and glasses with a range of compositions across eruption samples. More sodium rich plagioclase was identified via XRD in ash samples from Tungurahua, Mount Pinatubo and Eyjafjallajökull. More calcium rich plagioclase was identified in ash samples from Mount Saint Helens and Pacaya. Pyroxenes were identified in ash from Tungurahua and Mount Saint Helens. Apatite was identified in ash from Eyjafjallajökull, Mount Saint Helens, and Mount Pinatubo.

Analyses of pumice and scoria from the 1991 Pinatubo eruption done by Pallister and colleagues (1992) found accessory olivine and quartz present, indicating a state of disequilibrium. Olivine was not identified in that study by SEM or XRD. However, this does not mean it was not present at all. It is possible that it existed in very small amounts. Analyses of Pinatubo ash via XRD indicated the presence of calcian albite, quartz, hornblende, and anhydrite. Evidence of quartz, apatite, and plagioclase were also supported by SEM analysis. EDX analysis suggested that the calcain albite in the Pinatubo ash was near the composition of oligoclase. These phases were reported in other studies (Pallister et al., 1992; Jakubowski et al., 2002).

Analysis of Mount Saint Helens ash on the SEM showed evidence of plagioclase crystals and glasses with composition near laboradorite. X-ray Diffraction results for plagioclase present best matched with sodian anorthite. It is possible that glasses and crystals exist within a range of composition from labradorite to anorthite. X-ray Diffraction analysis of Mount Saint Helens ash indicates that pigeonite and quartz were also present. SEM analysis also provides support of their presence. Others have found plagioclase, hornblende, and pyroxenes (Pallister 1991; Farlow et al, 2012)

Analysis of Pacaya ash via XRD resulted in all major peaks being matched by sodian anorthite. SEM analysis showed evidence of iron hydroxides on the surface of glasses and some features with a composition similar to bytownite. Other studies have found plagioclase, olivine, and pyroxene (Bollasnia 2014; Hernandez personal communication 2020).

Tungurahua XRD analysis indicated the presence of albite, pigeonite, and augite. Evidence for pigeonite and plagioclase were found on the SEM. Analysis of Tungurahua ash and rock by others has reported plagioclase, pyroxenes, and Fe-Ti oxides present (Nauret et al., 2018).

X-ray diffraction of Eyjafjallajökull ash matched major peaks for anorthoclase and Sr bearing apatite. SEM analysis supported the finding of plagioclase and glass. It has been determined by

others that ash from the same eruption contained mostly andesitic glass, with the most abundant mineral being plagioclase. Pyroxenes and olivine were also observed (Gislason et al., 2010).

Dissolution rates and iron oxidizing bacteria

The addition of iron oxidizing bacteria did not have an apparent effect on the dissolution of silica or phosphate in these experiments. The bacteria used in these experiments are neutrophilic and microaerophilic. It is possible that bacteria existed on samples, however, it was not observed via SEM. It is also possible that the bacteria observed died in solution above the ash, settled to the bottom over time. It is unknown how much of the bacteria survived since no quantitative measurements were taken regarding their growth.

In experiments at lower pH done on more mafic material, the addition of iron oxidizing bacteria greatly inhibited dissolution (Santelli et al., 2001). Ashes are composed of minerals and glasses. The surfaces of these ashes are not all equally reactive. Silica-rich glasses dissolve orders of magnitude faster than minerals of comparable composition (Wolf-Boenisch et al., 2005). Key sites of dissolution can be covered by the bacterially mediated precipitation of iron oxyhydroxides.

Release rates of silica for andesitic ashes increase with decreasing pH (Kump and Brantley, 2000). It is possible that a combination of relatively slow dissolution and slow, or zero growth of bacteria worked together to make the difference between abiotic and biotic release rates negligible.

Cation release and context for the global carbon cycle

The release of Ca and Mg cations into water systems is important for the eventual precipitation of calcite and dolomite, which sequester carbon dioxide (Berner et al., 1983; Berner, 1999). In this experiment, although silica was released continuously, the concentration of free calcium increased slightly initially, and then remained constant. Silica dissolution was originally meant to be used as a proxy for the dissolution of Ca-Mg Silicate minerals and glasses, however, that may not be a reliable method in this case. In previous dissolution experiments preformed on volcanic ashes, initial concentrations of dissolved calcium, magnesium, and sodium, were attributed to the rapid dissolution of surface salts (Olsson et al., 2013). The release rates of key metals, including calcium, magnesium, and iron, in basic and acidic conditions vary exponentially based on the silica content of the glasses being weathered. Release rates are drastically slower with increasing silica content (Wolff-Boenisch et al., 2004). The silica and calcium content of glass are major controls on thermodynamic stability of glasses (Perrett et al., 2003).

CONCLUSIONS

In near neutral pH solutions, with and without marine salts, basaltic andesitic to trachy-dacitic ashes, when normalized for surface area, weather at comparable rates. Concentrations of dissolved silica increased over time for all ash samples. Concentrations of dissolved phosphate remained low and approximately constant over time. The first two weeks of the experiment yielded the highest release rates of Si. The presence of iron oxidizing bacteria did not alter any overall weathering trends. However, the effect of iron-oxidizing bacteria has on weathering rates of andesitic ashes was not conclusive in this study due to lack of evidence that the bacteria added survived, and absence of growth measurements.

Minerology determined by X-ray diffraction and SEM imaging were consistent with previous investigation of mineralogy of ashes from the same eruptions. SEM analysis at the conclusion of dissolution experiments showed alteration of pyroxenes on ash from Eyjafjallajökull and Tungurahua. Evidence of bacteria was found on ash from Mt. St. Helens and Pacaya.

RECOMMENDATIONS FOR FUTURE WORK

Since bacterial growth was not well documented in this study, in future work it should be measured periodically, perhaps with growth curves or fluorescence microscopy. The bacteria used were aerotactic and prefer low concentrations of oxygen; it is possible dissolved oxygen was too high in the experiments and no growth occurred. Therefore, measuring dissolved oxygen could be useful. Adding carbon dioxide to the system to enhance growth could aid in illuminating the effect of the bacteria on weathering rates.

Growth of bacteria are not uniformly distributed throughout environments with chemical gradients. A shaker table could be used to continually mix samples at regular time intervals. This would aid in dispersion of microsites of bacterial activity, electron donors and acceptors, and homogenize water chemistry.

Phosphate concentration measurements were low throughout the experiments. In the future, it would be of use to run samples multiple times to better determine error present in each measurement. Final phosphate concentrations were not able to be measured due to issues with the Skalar San++ nutrient analyzer and then an ensuing pandemic. In the future, samples could be re- analyzed.

Dissolved iron was not successfully detected in these experiments via the ferrozine method. To amend the limit of detection issue, dissolved iron concentrations could instead be measured via ICPMS.

Geochemical modeling by PHREEQ could aid in understanding controls on dissolution and precipitation by modeling saturation states.

REFERENCES CITED

Berner, R.A. (1999) A new look at the long-term carbon cycle, *GSA Today*, v. 9, 2-6.

Berner, R.A., Lasaga, A. and Garrells, R. (1983) The carbonate-silicate geochemical cycle and its effect on atmospheric carbon dioxide over the past 100 million years. *Am. J. Sci*. 283. 10.2475/ajs.283.7.641.

Best, M. G. (2001) *Igneous Petrology*. Malden, Mass. Blackwell Science

Cashman, K. and McConnell, S., (2005) Multiple levels of magma storage during the 1980 summer eruptions of Mount St. Helens, WA. *Bull. Vocanol*. 68, 57-75.

Carey, A. E., Kao, S.-J., Hicks, D. M., Nezat, C. A. and Lyons, W. B. (2005) The geochemistry of rivers in tectonically active areas of Taiwan and New Zealand. In *Tectonics, Climate and Landscape Evolution* (eds. S. D. Willett, N. Hovius, M. T. Brandon and D. M. Fisher). Special GSA Paper, vol. 398, pp. 339–351.

Carey, A. E., Nezat C. A., Lyons W. B., Kao S.-J. and Owen J. S. (2002) Trace metal fluxes to the ocean: the importance of highstanding islands. *Geophys. Res. Lett*. 29(23), 2099. doi:10.1029/ 2002GL015690.

Chapman, Thordarson. "Outline of Geology of Iceland." Https://Www.agu.org, 2012, www.agu.org/meetings/chapman/2012/bcall/pdf/Chapman_Outline_of_Geology_of_Iceland.pdf

Conway, M., Diehl, J., Matias, O. (1992) Paleomagnetic constraints on eruption patterns at the Pacaya composite volcano, Guatemala. *Bull. Volcanol*. 55, 25-32.

De la Cruz-Reyna, S., Tarraga, M., Ortiz, R., and Martinez-Bringas, A. (2010) Tectonic earthquakes triggering volcanic seismicity and eruptions. Case studies at Tungurahua and Popocatepetl volcanoes. *J. Vol. Geotherm. Res*.193, 37-48.

Farlow, N., Oberbeck, V., Snetsinger, K., Ferry, G., Polkowski, G., and Hayes, D. (1981) Size Distributions and Mineralogy of Ash Particles in the Stratosphere from Eruptions of Mount St. Helens. AAAS. 211, No. 4484, 832-834.

Fero, J., Carey, S., and Merrill, J. (2008) Simulation of the 1980 eruption of Mount St. Helens using the ash-tracking model PUFF. *J. Volcan. Geotherm. Res*. 175, 355-366.

Gislason, S., and Alfredsson H. (2010) Sampling the Volcanic Ash from the Eyjafjallajokull Volcano, Iceland- A Personal Account. *Elements* 4, 269-270.

Global Volcanism Program (2013) Eyjafjallajokull (372020) in Volcanoes of the World, v. 4.7.4. Venzke, E (ed.). Smithsonian Institution. Downloaded 29 Nov 2018 (https://volcano.si.edu/volcano.cfm?vn=372020). https://doi.org/10.5479/si.GVP.VOTW4-2013

Goldsmith, S. T., Carey, A. E., Johnson, B. M., Welch, S. A., Lyons, W. B., and McDowell, W. H. (2010) Stream geochemistry, chemical weathering and CO_2 consumption potential of andesitic terrains, Dominica, Lesser Antilles. *Geochim. Cosmochim. Acta* 74, 85–103. doi:10.1016/j.gca.2009.10.009.

IPCC (2014) Climate Change 2014: Synthesis Report. Contribution of Working Groups I, II and III to the Fifth Assessment Report of the Intergovernmental Panel on Climate Change

[Core Writing Team, R.K. Pachauri and L.A. Meyer (eds.)]. IPCC, Geneva, Switzerland, 151 pp.

Karl, D. M., Knauer, G. A. and Martin, J. H. (1988) Downward Flux of Particulate Organic Matter in the Ocean: A Particle Decomposition Paradox. *Nature News*. Nature Publishing Group, 31 Mar. 1988. Web.

Keiding, J., and Sigmarsson, O. (2012) Geothermobarometry of the 2010 Eyjafjallajokull eruption: New constraints on Icelandic magma plumbing systems. *J. Geophys. Res.-Solid Earth* 117, Article Number: B00C09.

NERC (2018). Changing eruption styles at Eyjafjallajökull in Iceland. Retrieved from https://www.bgs.ac.uk/research/volcanoes/changingEruptionstyles.html

Pierson, T., Janda, R., Umbal, J., Daag, J., 1992. Immediate and long-tern hazards from lahars and excess sedimentation in rivers draining Mt. Pinatubo, Philippines. Vancouver: US Geological Survey, 1-8.

Portier, A. (2012) Dissolution Kinetics of Andesitic-Dacitic Ash, The Ohio State University. School of Earth Sciences Honors Thesis.

Santelli, C. M., Welch, S. A., Westrich, H. R., and Banfield, J. F. (2001) The effect of Fe-oxidizing bacteria on Fe-silicate mineral dissolution, *Chemical Geology*, Volume 180, 2001, pp. 99-115.

Schopka, H. H., Derry, L. A., & Arcilla, C. A. (2011) Chemical weathering, river geochemistry and atmospheric carbon fluxes from volcanic and ultramafic regions on Luzon Island, the Philippines. *Geochimica et Cosmochimica Acta*, 75(4), 978–1002. https://doi.org/10.1016/j.gca.2010.11.014

Singer, E., Emerson, D., Webb, E. A., Barco, R. A., Kuenen, J. G., Nelson, W. C., Chan, C. S., Comolli, L. R., Ferriera, S., Johnson, J., Heidelberg, J. F., & Edwards, K. J. (2011). Mariprofundus ferrooxydans PV-1 the first genome of a marine Fe(II) oxidizing Zetaproteobacterium. *PloS One*, 6(9), e25386. https://doi.org/10.1371/journal.pone.0025386

Stookey, L. (1970) Ferrozine-A new spectrophotometric reagent for iron. *Analytical Chemistry* 42, 79-81.

Thordarson, Thorvaldur & Hoskuldsson, Armann. (2008). Postglacial volcanism in Iceland. Jökull. 58.

United Nations Guatemala Relief Report (2010). https://reliefweb.int/sites/reliefweb.int/files/resources/88DB1DFC068AAF808525779E00715947-Full_Appeal.pdf

APPENDIX

CATION SUMMARY REPORT

No.	Name	Time min Lithium ECD_1	Area µS*min Lithium ECD_1	Rel.Area % Lithium ECD_1	Height µS Lithium ECD_1	Rel.Height % Lithium ECD_1	Amount Lithium ECD_1
1	IC	n.a.	n.a.	n.a.	n.a.	n.a.	n.a.
2	q	n.a.	n.a.	n.a.	n.a.	n.a.	n.a.
3	STD B	2.833	0.0007	0.64	0.01	1.36	0.7244
4	STD 1	2.847	0.0041	0.89	0.03	2.05	0.7933
5	STD 2	2.864	0.0089	1.00	0.05	2.39	0.8672
6	STD 3	2.870	0.0231	1.19	0.12	2.89	0.8958
7	STD 4	2.890	0.0486	1.39	0.23	3.19	0.9426
8	STD 5	2.910	0.1041	1.34	0.48	2.71	1.0090
9	STD 6	2.907	0.2586	1.32	1.11	1.78	1.0022
10	STOCK STD	2.883	0.4954	1.12	1.88	1.30	0.9602
11	CHECK STD (sUB IN STOCK)	2.927	0.2871	8.15	1.32	13.81	0.5564
12	usgs	n.a.	n.a.	n.a.	n.a.	n.a.	n.a.
13	TAP	2.830	0.0011	0.01	0.01	0.03	0.0021
14	TAP	2.827	0.0010	0.01	0.01	0.03	0.0019
15	5	2.890	0.1202	1.57	0.66	2.90	0.2330
16	6	2.904	0.2902	1.28	1.30	1.89	0.5624
17	STOCK	2.880	0.6363	1.29	2.26	1.48	1.2332
18	CHECK	2.924	0.2971	8.28	1.38	14.29	0.5759
19	Q	2.850	0.0003	0.00	0.00	0.00	0.0006
20	PIN A JAN7	2.827	0.0001	0.00	0.00	0.00	0.0002
21	PAC A JAN 7	2.857	0.0001	0.00	0.00	0.00	0.0001
22	TUN A JAN7	2.864	0.0001	0.00	0.00	0.00	0.0001
23	MSH A JAN7	2.877	0.0000	0.00	0.00	0.00	0.0001
24	ICE A JAN7	2.847	0.0002	0.00	0.00	0.00	0.0004
25	ICE B JAN 7	2.853	0.0002	0.00	0.00	0.00	0.0004
26	PIN B JAN 7	2.847	0.0001	0.00	0.00	0.00	0.0001
27	PAC B JAN 7	2.894	0.0001	0.00	0.00	0.00	0.0002
28	TUN B JAN 7	2.844	0.0001	0.00	0.00	0.00	0.0002
29	MSH B JAN7	2.877	0.0001	0.00	0.00	0.00	0.0002
30	ICE B JAN 7	2.867	0.0002	0.00	0.00	0.00	0.0004
31	ICE A SEP95.2018	2.847	0.0002	0.00	0.00	0.00	0.0003
32	PAC A SEP5.2018	n.a.	n.a.	n.a.	n.a.	n.a.	n.a.
33	PIN A SEP5.2018	2.847	0.0001	0.00	0.00	0.00	0.0002
34	TUN A SEP5.2018	n.a.	n.a.	n.a.	n.a.	n.a.	n.a.
35	MSH A SEP5.2018	2.833	0.0001	0.00	0.00	0.00	0.0001
36	FRESHBASE	n.a.	n.a.	n.a.	n.a.	n.a.	n.a.
37	ICE B SEP 5. 2018	2.860	0.0002	0.00	0.00	0.00	0.0004
38	PAC B SEP 5.2018	n.a.	n.a.	n.a.	n.a.	n.a.	n.a.

39	PIN B SEP 5.2018	2.890	0.0001	0.00	0.00	0.00	0.0001
40	TUN B SEP5.2018	2.874	0.0000	0.00	0.00	0.00	0.0001
41	MSH B SEP5.2018	2.863	0.0001	0.00	0.00	0.00	0.0002
42	FRESH BASE 2	n.a.	n.a.	n.a.	n.a.	n.a.	n.a.
43	ICE A 7/19/2018	2.860	0.0001	0.00	0.00	0.00	0.0003
44	PAC A 7/19/2018	n.a.	n.a.	n.a.	n.a.	n.a.	n.a.
45	PIN A 7/19/2018	2.837	0.0001	0.00	0.00	0.00	0.0001
46	TUN A 7/19/2018	n.a.	n.a.	n.a.	n.a.	n.a.	n.a.
47	MSH A 7/19/2018	2.887	0.0001	0.00	0.00	0.00	0.0002
48	MIILIQ	n.a.	n.a.	n.a.	n.a.	n.a.	n.a.
49	ICE B 7/19/2018	2.873	0.0001	0.00	0.00	0.00	0.0002
50	PAC B 7/19/2018	n.a.	n.a.	n.a.	n.a.	n.a.	n.a.
51	PIN B 7/19/2018	2.854	0.0001	0.00	0.00	0.00	0.0002
52	TUN B 7/19/2018	n.a.	n.a.	n.a.	n.a.	n.a.	n.a.
53	MSH B 7/19/2018	2.887	0.0000	0.00	0.00	0.00	0.0001
54	FRESHBASE 3	n.a.	n.a.	n.a.	n.a.	n.a.	n.a.
55	Q	n.a.	n.a.	n.a.	n.a.	n.a.	n.a.
56	Q	n.a.	n.a.	n.a.	n.a.	n.a.	n.a.
57	Q	n.a.	n.a.	n.a.	n.a.	n.a.	n.a.
58	Q	n.a.	n.a.	n.a.	n.a.	n.a.	n.a.
59	Q	n.a.	n.a.	n.a.	n.a.	n.a.	n.a.
60	Q	n.a.	n.a.	n.a.	n.a.	n.a.	n.a.
61	Q	n.a.	n.a.	n.a.	n.a.	n.a.	n.a.
62	Q	n.a.	n.a.	n.a.	n.a.	n.a.	n.a.
63	Q	n.a.	n.a.	n.a.	n.a.	n.a.	n.a.
64	Q	n.a.	n.a.	n.a.	n.a.	n.a.	n.a.
65	Q	n.a.	n.a.	n.a.	n.a.	n.a.	n.a.
66	Q	n.a.	n.a.	n.a.	n.a.	n.a.	n.a.
67	Q	n.a.	n.a.	n.a.	n.a.	n.a.	n.a.
68	Q	n.a.	n.a.	n.a.	n.a.	n.a.	n.a.
69	Q	n.a.	n.a.	n.a.	n.a.	n.a.	n.a.
70	Q	n.a.	n.a.	n.a.	n.a.	n.a.	n.a.
71	Q	n.a.	n.a.	n.a.	n.a.	n.a.	n.a.
	Sum:	114.697	2.579	29.490	10.865	52.105	10.365
	Average:	2.867	0.064	0.737	0.272	1.303	0.259
	Rel.Std.Dev:	0.911 %	226.776 %	247.044 %	212.400 %	240.797 %	156.189 %

No.	Name	Time min Sodium ECD_1	Area µS*min Sodium ECD_1	Rel.Area % Sodium ECD_1	Height µS Sodium ECD_1	Rel.Height % Sodium ECD_1	Amount Sodium ECD_1
1	IC	3.35	0.002	4.10	0.011	8.88	0.0107
2	q	3.34	0.000	1.27	0.002	2.78	0.0022
3	STD B	3.39	0.032	27.53	0.155	41.11	90.6253
4	STD 1	3.48	0.175	37.86	0.541	41.09	99.0547

5	STD 2	3.55	0.364	40.90	0.896	40.00	103.1202
6	STD 3	3.59	0.906	46.57	1.792	43.32	102.6111
7	STD 4	3.52	1.811	51.79	3.777	52.81	102.5029
8	STD 5	3.41	3.558	45.74	11.721	66.01	100.6972
9	STD 6	3.39	8.812	45.14	42.554	67.85	99.7578
10	STOCK STD	3.38	18.435	41.67	91.494	63.24	104.3510
11	CHECK STD (sUB IN STOCK)	3.44	0.371	10.53	1.744	18.26	2.0994
12	usgs	3.41	5.298	34.07	23.554	60.71	29.9916
13	TAP	3.41	3.386	30.64	13.926	53.80	19.1648
14	TAP	3.41	3.085	28.33	12.389	50.22	17.4616
15	5	3.40	3.747	48.85	15.734	68.69	21.2077
16	6	3.39	9.363	41.37	45.702	66.25	53.0012
17	STOCK	3.38	19.457	39.41	94.780	62.08	110.1390
18	CHECK	3.43	0.380	10.60	1.810	18.75	2.1531
19	Q	3.50	41.572	98.46	217.849	99.27	235.3196
20	PIN A JAN7	3.50	41.140	98.36	215.006	99.37	232.8795
21	PAC A JAN 7	3.50	41.487	99.26	217.047	99.65	234.8397
22	TUN A JAN7	3.51	41.442	99.55	218.509	99.77	234.5865
23	MSH A JAN7	3.51	41.640	99.63	217.440	99.82	235.7068
24	ICE A JAN7	3.50	40.488	98.43	215.311	99.29	229.1855
25	ICE B JAN 7	3.51	40.842	98.34	215.984	99.25	231.1882
26	PIN B JAN 7	3.51	41.405	98.49	212.390	99.41	234.3779
27	PAC B JAN 7	3.53	42.857	99.24	219.097	99.63	242.5983
28	TUN B JAN 7	3.53	42.350	99.22	216.276	99.60	239.7273
29	MSH B JAN7	3.53	41.574	99.21	214.759	99.61	235.3320
30	ICE B JAN 7	3.53	41.287	98.34	214.746	99.26	233.7083
31	ICE A SEP95.2018	3.52	41.928	98.58	218.629	99.33	237.3392
32	PAC A SEP5.2018	3.50	42.496	99.67	217.804	99.84	240.5523
33	PIN A SEP5.2018	3.52	44.791	99.30	226.909	99.68	253.5426
34	TUN A SEP5.2018	3.52	45.038	99.65	227.546	99.82	254.9437
35	MSH A SEP5.2018	3.51	42.390	99.29	218.480	99.67	239.9550
36	FRESHBASE	3.47	22.365	99.71	114.216	99.86	126.5979
37	ICE B SEP 5. 2018	3.52	41.419	98.56	216.643	99.39	234.4555
38	PAC B SEP 5.2018	3.53	43.432	99.44	219.944	99.71	245.8525
39	PIN B SEP 5.2018	3.56	53.735	95.14	266.976	98.23	304.1738
40	TUN B SEP5.2018	3.55	44.591	98.91	228.141	99.43	252.4093
41	MSH B SEP5.2018	3.53	42.914	99.27	219.781	99.63	242.9195
42	FRESH BASE 2	3.48	30.429	99.87	157.808	99.94	172.2478
43	ICE A 7/19/2018	3.52	42.546	98.59	217.868	99.30	240.8378
44	PAC A 7/19/2018	3.52	42.592	99.61	217.730	99.81	241.0970
45	PIN A 7/19/2018	3.52	42.191	98.55	215.224	99.38	238.8241
46	TUN A 7/19/2018	3.52	43.225	99.63	220.404	99.81	244.6784
47	MSH A 7/19/2018	3.53	43.176	99.06	220.201	99.56	244.4016
48	MIILIQ	3.43	0.013	12.64	0.063	14.05	0.0711
49	ICE B 7/19/2018	3.53	42.479	98.47	217.476	99.31	240.4546

50	PAC B 7/19/2018	3.54	43.185	99.12	220.318	99.56	244.4524
51	PIN B 7/19/2018	3.56	50.155	98.86	254.386	99.46	283.9071
52	TUN B 7/19/2018	3.52	42.784	98.80	221.087	99.41	242.1808
53	MSH B 7/19/2018	3.52	43.990	98.92	226.034	99.48	249.0067
54	FRESHBASE 3	3.51	34.539	99.90	179.529	99.95	195.5099
55	Q	3.54	2.073	97.88	4.277	95.95	11.7327
56	Q	n.a.	n.a.	n.a.	n.a.	n.a.	n.a.
57	Q	3.55	0.507	76.02	1.136	58.73	2.8695
58	Q	3.51	0.190	91.81	0.518	90.94	1.0776
59	Q	3.47	0.103	100.00	0.306	100.00	0.5830
60	Q	3.45	0.058	100.00	0.180	100.00	0.3301
61	Q	3.44	0.034	100.00	0.107	100.00	0.1949
62	Q	3.41	0.021	84.86	0.065	96.90	0.1194
63	Q	3.41	0.013	100.00	0.040	100.00	0.0759
64	Q	3.41	0.009	100.00	0.026	100.00	0.0510
65	Q	3.39	0.006	100.00	0.017	100.00	0.0338
66	Q	3.40	0.004	100.00	0.012	100.00	0.0230
67	Q	3.38	0.003	100.00	0.011	100.00	0.0191
68	Q	3.39	0.002	42.90	0.008	66.43	0.0134
69	Q	3.37	0.002	100.00	0.007	100.00	0.0104
70	Q	3.42	0.023	100.00	0.119	100.00	0.1323
71	Q	3.40	0.002	100.00	0.010	100.00	0.0116
	Sum:	243.211	1,546.721	5,555.925	7,907.032	5,832.306	9,365.089
	Average:	3.474	22.096	79.370	112.958	83.319	133.787
	Rel.Std.Dev:	1.802 %	92.608 %	39.592 %	93.673 %	32.671 %	82.209 %

No.	Name	Time min Ammonium ECD_1	Area µS*min Ammonium ECD_1	Rel.Area % Ammonium ECD_1	Height µS Ammonium ECD_1	Rel.Height % Ammonium ECD_1	Amount Ammonium ECD_1
1	IC	n.a.	n.a.	n.a.	n.a.	n.a.	n.a.
2	q	n.a.	n.a.	n.a.	n.a.	n.a.	n.a.
3	STD B	n.a.	n.a.	n.a.	n.a.	n.a.	n.a.
4	STD 1	n.a.	n.a.	n.a.	n.a.	n.a.	n.a.
5	STD 2	n.a.	n.a.	n.a.	n.a.	n.a.	n.a.
6	STD 3	n.a.	n.a.	n.a.	n.a.	n.a.	n.a.
7	STD 4	n.a.	n.a.	n.a.	n.a.	n.a.	n.a.
8	STD 5	n.a.	n.a.	n.a.	n.a.	n.a.	n.a.
9	STD 6	n.a.	n.a.	n.a.	n.a.	n.a.	n.a.
10	STOCK STD	n.a.	n.a.	n.a.	n.a.	n.a.	n.a.
11	CHECK STD (sUB IN STOCK)	3.940	0.640	18.171	2.279	23.863	n.a.
12	usgs	n.a.	n.a.	n.a.	n.a.	n.a.	n.a.
13	TAP	n.a.	n.a.	n.a.	n.a.	n.a.	n.a.
14	TAP	n.a.	n.a.	n.a.	n.a.	n.a.	n.a.

15	5	n.a.	n.a.	n.a.	n.a.	n.a.	n.a.
16	6	n.a.	n.a.	n.a.	n.a.	n.a.	n.a.
17	STOCK	n.a.	n.a.	n.a.	n.a.	n.a.	n.a.
18	CHECK	3.937	0.641	17.858	2.334	24.182	n.a.
19	Q	n.a.	n.a.	n.a.	n.a.	n.a.	n.a.
20	PIN A JAN7	n.a.	n.a.	n.a.	n.a.	n.a.	n.a.
21	PAC A JAN 7	n.a.	n.a.	n.a.	n.a.	n.a.	n.a.
22	TUN A JAN7	n.a.	n.a.	n.a.	n.a.	n.a.	n.a.
23	MSH A JAN7	n.a.	n.a.	n.a.	n.a.	n.a.	n.a.
24	ICE A JAN7	n.a.	n.a.	n.a.	n.a.	n.a.	n.a.
25	ICE B JAN 7	n.a.	n.a.	n.a.	n.a.	n.a.	n.a.
26	PIN B JAN 7	n.a.	n.a.	n.a.	n.a.	n.a.	n.a.
27	PAC B JAN 7	n.a.	n.a.	n.a.	n.a.	n.a.	n.a.
28	TUN B JAN 7	n.a.	n.a.	n.a.	n.a.	n.a.	n.a.
29	MSH B JAN7	n.a.	n.a.	n.a.	n.a.	n.a.	n.a.
30	ICE B JAN 7	n.a.	n.a.	n.a.	n.a.	n.a.	n.a.
31	ICE A SEP95.2018	n.a.	n.a.	n.a.	n.a.	n.a.	n.a.
32	PAC A SEP5.2018	n.a.	n.a.	n.a.	n.a.	n.a.	n.a.
33	PIN A SEP5.2018	n.a.	n.a.	n.a.	n.a.	n.a.	n.a.
34	TUN A SEP5.2018	n.a.	n.a.	n.a.	n.a.	n.a.	n.a.
35	MSH A SEP5.2018	n.a.	n.a.	n.a.	n.a.	n.a.	n.a.
36	FRESHBASE	n.a.	n.a.	n.a.	n.a.	n.a.	n.a.
37	ICE B SEP 5. 2018	n.a.	n.a.	n.a.	n.a.	n.a.	n.a.
38	PAC B SEP 5.2018	n.a.	n.a.	n.a.	n.a.	n.a.	n.a.
39	PIN B SEP 5.2018	n.a.	n.a.	n.a.	n.a.	n.a.	n.a.
40	TUN B SEP5.2018	n.a.	n.a.	n.a.	n.a.	n.a.	n.a.
41	MSH B SEP5.2018	n.a.	n.a.	n.a.	n.a.	n.a.	n.a.
42	FRESH BASE 2	n.a.	n.a.	n.a.	n.a.	n.a.	n.a.
43	ICE A 7/19/2018	n.a.	n.a.	n.a.	n.a.	n.a.	n.a.
44	PAC A 7/19/2018	n.a.	n.a.	n.a.	n.a.	n.a.	n.a.
45	PIN A 7/19/2018	n.a.	n.a.	n.a.	n.a.	n.a.	n.a.
46	TUN A 7/19/2018	n.a.	n.a.	n.a.	n.a.	n.a.	n.a.
47	MSH A 7/19/2018	n.a.	n.a.	n.a.	n.a.	n.a.	n.a.
48	MIILIQ	3.787	0.021	21.292	0.064	14.215	n.a.
49	ICE B 7/19/2018	n.a.	n.a.	n.a.	n.a.	n.a.	n.a.
50	PAC B 7/19/2018	n.a.	n.a.	n.a.	n.a.	n.a.	n.a.
51	PIN B 7/19/2018	n.a.	n.a.	n.a.	n.a.	n.a.	n.a.
52	TUN B 7/19/2018	n.a.	n.a.	n.a.	n.a.	n.a.	n.a.
53	MSH B 7/19/2018	n.a.	n.a.	n.a.	n.a.	n.a.	n.a.
54	FRESHBASE 3	n.a.	n.a.	n.a.	n.a.	n.a.	n.a.
55	Q	n.a.	n.a.	n.a.	n.a.	n.a.	n.a.
56	Q	n.a.	n.a.	n.a.	n.a.	n.a.	n.a.
57	Q	n.a.	n.a.	n.a.	n.a.	n.a.	n.a.

58	Q	n.a.	n.a.	n.a.	n.a.	n.a.	n.a.
59	Q	n.a.	n.a.	n.a.	n.a.	n.a.	n.a.
60	Q	n.a.	n.a.	n.a.	n.a.	n.a.	n.a.
61	Q	n.a.	n.a.	n.a.	n.a.	n.a.	n.a.
62	Q	n.a.	n.a.	n.a.	n.a.	n.a.	n.a.
63	Q	n.a.	n.a.	n.a.	n.a.	n.a.	n.a.
64	Q	n.a.	n.a.	n.a.	n.a.	n.a.	n.a.
65	Q	n.a.	n.a.	n.a.	n.a.	n.a.	n.a.
66	Q	n.a.	n.a.	n.a.	n.a.	n.a.	n.a.
67	Q	n.a.	n.a.	n.a.	n.a.	n.a.	n.a.
68	Q	n.a.	n.a.	n.a.	n.a.	n.a.	n.a.
69	Q	n.a.	n.a.	n.a.	n.a.	n.a.	n.a.
70	Q	n.a.	n.a.	n.a.	n.a.	n.a.	n.a.
71	Q	n.a.	n.a.	n.a.	n.a.	n.a.	n.a.
	Sum:	11.664	1.302	57.321	4.677	62.260	0.000
	Average:	3.888	0.434	19.107	1.559	20.753	#DIV/0!
	Rel.Std.Dev:	2.255 %	82.382 %	9.938 %	83.069 %	27.294 %	#DIV/0!

No.	Name	Time min Potassium ECD_1	Area µS*min Potassium ECD_1	Rel.Area % Potassium ECD_1	Height µS Potassium ECD_1	Rel.Height % Potassium ECD_1	Amount Potassium ECD_1
1	IC	4.567	0.003	7.534	0.010	8.529	0.031
2	q	4.624	0.001	2.722	0.003	3.277	0.007
3	STD B	4.720	0.002	1.931	0.009	2.286	9.937
4	STD 1	4.750	0.013	2.811	0.059	4.452	11.499
5	STD 2	4.790	0.031	3.535	0.132	5.898	13.935
6	STD 3	4.810	0.093	4.798	0.324	7.820	16.529
7	STD 4	4.847	0.201	5.743	0.624	8.731	17.771
8	STD 5	4.857	0.435	5.589	1.357	7.641	19.238
9	STD 6	4.820	1.145	5.864	3.438	5.481	20.259
10	STOCK STD	4.757	2.388	5.398	7.511	5.192	21.134
11	CHECK STD (sUB IN STOCK)	4.804	0.334	9.491	1.258	13.175	2.959
12	usgs	4.830	0.559	3.597	2.053	5.292	4.950
13	TAP	4.810	0.469	4.245	1.851	7.151	4.151
14	TAP	4.813	0.489	4.491	1.905	7.721	4.328
15	5	4.807	0.462	6.031	1.823	7.960	4.093
16	6	4.800	1.211	5.352	3.951	5.727	10.719
17	STOCK	4.747	2.607	5.281	8.156	5.342	23.075
18	CHECK	4.790	0.301	8.383	1.200	12.432	2.662
19	Q	4.780	0.060	0.142	0.308	0.140	0.530
20	PIN A JAN7	4.764	0.020	0.047	0.102	0.047	0.175
21	PAC A JAN 7	n.a.	n.a.	n.a.	n.a.	n.a.	n.a.

22	TUN A JAN7	4.770	0.011	0.027	0.060	0.027	0.101
23	MSH A JAN7	n.a.	n.a.	n.a.	n.a.	n.a.	n.a.
24	ICE A JAN7	4.817	0.049	0.119	0.216	0.100	0.432
25	ICE B JAN 7	4.827	0.042	0.100	0.195	0.090	0.369
26	PIN B JAN 7	4.680	0.011	0.025	0.000	0.000	0.094
27	PAC B JAN 7	n.a.	n.a.	n.a.	n.a.	n.a.	n.a.
28	TUN B JAN 7	4.834	0.022	0.052	0.102	0.047	0.198
29	MSH B JAN7	4.840	0.023	0.056	0.104	0.048	0.207
30	ICE B JAN 7	4.860	0.038	0.090	0.161	0.074	0.336
31	ICE A SEP95.2018	4.850	0.038	0.090	0.168	0.076	0.341
32	PAC A SEP5.2018	n.a.	n.a.	n.a.	n.a.	n.a.	n.a.
33	PIN A SEP5.2018	n.a.	n.a.	n.a.	n.a.	n.a.	n.a.
34	TUN A SEP5.2018	n.a.	n.a.	n.a.	n.a.	n.a.	n.a.
35	MSH A SEP5.2018	4.770	0.005	0.011	0.002	0.001	0.042
36	FRESHBASE	n.a.	n.a.	n.a.	n.a.	n.a.	n.a.
37	ICE B SEP 5. 2018	4.763	0.020	0.047	0.002	0.001	0.175
38	PAC B SEP 5.2018	n.a.	n.a.	n.a.	n.a.	n.a.	n.a.
39	PIN B SEP 5.2018	4.997	0.225	0.398	0.603	0.222	1.990
40	TUN B SEP5.2018	4.847	0.023	0.051	0.122	0.053	0.203
41	MSH B SEP5.2018	4.827	0.021	0.048	0.100	0.045	0.182
42	FRESH BASE 2	n.a.	n.a.	n.a.	n.a.	n.a.	n.a.
43	ICE A 7/19/2018	4.844	0.053	0.122	0.235	0.107	0.465
44	PAC A 7/19/2018	n.a.	n.a.	n.a.	n.a.	n.a.	n.a.
45	PIN A 7/19/2018	n.a.	n.a.	n.a.	n.a.	n.a.	n.a.
46	TUN A 7/19/2018	n.a.	n.a.	n.a.	n.a.	n.a.	n.a.
47	MSH A 7/19/2018	4.704	0.017	0.039	0.000	0.000	0.151
48	MIILIQ	n.a.	n.a.	n.a.	n.a.	n.a.	n.a.
49	ICE B 7/19/2018	4.870	0.049	0.113	0.122	0.055	0.430
50	PAC B 7/19/2018	n.a.	n.a.	n.a.	n.a.	n.a.	n.a.
51	PIN B 7/19/2018	n.a.	n.a.	n.a.	n.a.	n.a.	n.a.
52	TUN B 7/19/2018	n.a.	n.a.	n.a.	n.a.	n.a.	n.a.
53	MSH B 7/19/2018	n.a.	n.a.	n.a.	n.a.	n.a.	n.a.
54	FRESHBASE 3	n.a.	n.a.	n.a.	n.a.	n.a.	n.a.
55	Q	4.770	0.022	1.062	0.106	2.385	0.199
56	Q	n.a.	n.a.	n.a.	n.a.	n.a.	n.a.
57	Q	n.a.	n.a.	n.a.	n.a.	n.a.	n.a.
58	Q	n.a.	n.a.	n.a.	n.a.	n.a.	n.a.
59	Q	n.a.	n.a.	n.a.	n.a.	n.a.	n.a.
60	Q	n.a.	n.a.	n.a.	n.a.	n.a.	n.a.
61	Q	n.a.	n.a.	n.a.	n.a.	n.a.	n.a.
62	Q	n.a.	n.a.	n.a.	n.a.	n.a.	n.a.
63	Q	n.a.	n.a.	n.a.	n.a.	n.a.	n.a.
64	Q	n.a.	n.a.	n.a.	n.a.	n.a.	n.a.

65	Q	n.a.	n.a.	n.a.	n.a.	n.a.	n.a.
66	Q	n.a.	n.a.	n.a.	n.a.	n.a.	n.a.
67	Q	n.a.	n.a.	n.a.	n.a.	n.a.	n.a.
68	Q	n.a.	n.a.	n.a.	n.a.	n.a.	n.a.
69	Q	n.a.	n.a.	n.a.	n.a.	n.a.	n.a.
70	Q	n.a.	n.a.	n.a.	n.a.	n.a.	n.a.
71	Q	n.a.	n.a.	n.a.	n.a.	n.a.	n.a.
	Sum:	177.353	11.493	95.436	38.370	127.627	193.894
	Average:	4.793	0.311	2.579	1.037	3.449	5.240
	Rel.Std.Dev:	1.526 %	194.962 %	111.671 %	184.137 %	113.651 %	141.203 %

No.	Name	Time min Magnesium ECD_1	Area µS*min Magnesium ECD_1	Rel.Area % Magnesium ECD_1	Height µS Magnesium ECD_1	Rel.Height % Magnesium ECD_1	Amount Magnesium ECD_1
1	IC	7.004	0.003	6.527	0.008	7.036	0.272
2	q	7.000	0.002	7.140	0.006	7.855	0.268
3	STD B	7.007	0.038	32.518	0.109	29.072	218.993
4	STD 1	7.020	0.161	34.810	0.437	33.203	102.373
5	STD 2	7.044	0.288	32.313	0.714	31.857	81.400
6	STD 3	7.003	0.528	27.124	1.131	27.335	55.412
7	STD 4	7.007	0.788	22.551	1.474	20.608	40.109
8	STD 5	7.097	1.730	22.237	2.227	12.541	42.458
9	STD 6	7.087	5.353	27.423	9.734	15.520	51.474
10	STOCK STD	6.990	13.754	31.089	28.940	20.004	65.725
11	CHECK STD (sUB IN STOCK)	7.034	0.510	14.483	1.148	12.019	2.687
12	usgs	7.157	2.411	15.509	3.310	8.532	11.737
13	TAP	7.037	0.965	8.732	1.721	6.649	4.850
14	TAP	7.043	0.917	8.426	1.696	6.875	4.625
15	5	7.147	1.826	23.812	2.696	11.770	8.950
16	6	7.094	6.415	28.344	11.038	16.000	30.791
17	STOCK	6.990	15.463	31.322	30.931	20.258	73.863
18	CHECK	7.044	0.539	15.020	1.220	12.644	2.823
19	Q	7.047	0.129	0.306	0.365	0.166	0.873
20	PIN A JAN7	7.040	0.024	0.058	0.073	0.034	0.373
21	PAC A JAN 7	7.057	0.084	0.202	0.249	0.114	0.660
22	TUN A JAN7	7.050	0.042	0.100	0.124	0.057	0.457
23	MSH A JAN7	7.050	0.027	0.065	0.081	0.037	0.388
24	ICE A JAN7	7.054	0.125	0.304	0.361	0.166	0.853
25	ICE B JAN 7	7.073	0.137	0.329	0.388	0.178	0.909
26	PIN B JAN 7	7.064	0.028	0.067	0.084	0.039	0.392
27	PAC B JAN 7	7.090	0.113	0.261	0.325	0.148	0.795
28	TUN B JAN 7	7.080	0.070	0.164	0.207	0.095	0.591

29	MSH B JAN7	7.084	0.069	0.164	0.203	0.094	0.585
30	ICE B JAN 7	7.083	0.136	0.324	0.385	0.178	0.904
31	ICE A SEP95.2018	7.050	0.128	0.302	0.369	0.168	0.869
32	PAC A SEP5.2018	7.027	0.028	0.065	0.084	0.038	0.391
33	PIN A SEP5.2018	7.037	0.019	0.043	0.058	0.026	0.350
34	TUN A SEP5.2018	7.044	0.048	0.105	0.140	0.061	0.484
35	MSH A SEP5.2018	7.047	0.080	0.188	0.234	0.107	0.639
36	FRESHBASE	7.040	0.013	0.057	0.038	0.033	0.319
37	ICE B SEP 5. 2018	7.063	0.117	0.278	0.336	0.154	0.815
38	PAC B SEP 5.2018	7.074	0.133	0.304	0.373	0.169	0.891
39	PIN B SEP 5.2018	7.094	1.461	2.587	2.523	0.928	7.212
40	TUN B SEP5.2018	7.094	0.303	0.673	0.806	0.351	1.701
41	MSH B SEP5.2018	7.063	0.074	0.171	0.215	0.098	0.609
42	FRESH BASE 2	7.020	0.009	0.030	0.027	0.017	0.301
43	ICE A 7/19/2018	7.037	0.139	0.322	0.391	0.178	0.920
44	PAC A 7/19/2018	7.030	0.032	0.075	0.097	0.044	0.411
45	PIN A 7/19/2018	7.047	0.066	0.154	0.195	0.090	0.572
46	TUN A 7/19/2018	7.044	0.047	0.109	0.139	0.063	0.483
47	MSH A 7/19/2018	7.057	0.135	0.309	0.377	0.171	0.900
48	MIILIQ	7.053	0.011	10.985	0.030	6.572	0.310
49	ICE B 7/19/2018	7.060	0.125	0.290	0.361	0.165	0.854
50	PAC B 7/19/2018	7.070	0.163	0.373	0.453	0.205	1.032
51	PIN B 7/19/2018	7.074	0.183	0.360	0.506	0.198	1.127
52	TUN B 7/19/2018	7.020	0.262	0.604	0.716	0.322	1.503
53	MSH B 7/19/2018	7.030	0.177	0.399	0.497	0.219	1.103
54	FRESHBASE 3	7.020	0.009	0.027	0.028	0.016	0.303
55	Q	7.014	0.006	0.277	0.017	0.376	0.286
56	Q	n.a.	n.a.	n.a.	n.a.	n.a.	n.a.
57	Q	7.304	0.007	1.083	0.038	1.969	0.292
58	Q	n.a.	n.a.	n.a.	n.a.	n.a.	n.a.
59	Q	n.a.	n.a.	n.a.	n.a.	n.a.	n.a.
60	Q	n.a.	n.a.	n.a.	n.a.	n.a.	n.a.
61	Q	n.a.	n.a.	n.a.	n.a.	n.a.	n.a.
62	Q	n.a.	n.a.	n.a.	n.a.	n.a.	n.a.
63	Q	n.a.	n.a.	n.a.	n.a.	n.a.	n.a.
64	Q	n.a.	n.a.	n.a.	n.a.	n.a.	n.a.
65	Q	n.a.	n.a.	n.a.	n.a.	n.a.	n.a.
66	Q	n.a.	n.a.	n.a.	n.a.	n.a.	n.a.
67	Q	n.a.	n.a.	n.a.	n.a.	n.a.	n.a.
68	Q	n.a.	n.a.	n.a.	n.a.	n.a.	n.a.
69	Q	n.a.	n.a.	n.a.	n.a.	n.a.	n.a.
70	Q	n.a.	n.a.	n.a.	n.a.	n.a.	n.a.
71	Q	n.a.	n.a.	n.a.	n.a.	n.a.	n.a.

	Sum:	395.082	56.450	411.897	110.434	313.823	831.268
	Average:	7.055	1.008	7.355	1.972	5.604	14.844
	Rel.Std.Dev:	0.677 %	286.662 %	154.909 %	293.232 %	163.327 %	245.314 %

No.	Name	Time min Calcium ECD_1	Area µS*min Calcium ECD_1	Rel.Area % Calcium ECD_1	Height µS Calcium ECD_1	Rel.Height % Calcium ECD_1	Amount Calcium ECD_1
1	IC	8.750	0.038	81.841	0.091	75.552	0.046
2	q	8.740	0.027	88.866	0.066	86.089	-0.019
3	STD B	8.753	0.037	31.649	0.088	23.432	19.679
4	STD 1	8.753	0.105	22.818	0.249	18.951	46.756
5	STD 2	8.774	0.198	22.243	0.445	19.860	52.281
6	STD 3	8.717	0.395	20.317	0.771	18.631	45.524
7	STD 4	8.727	0.643	18.396	1.045	14.606	38.216
8	STD 5	8.833	1.952	25.097	1.971	11.102	59.937
9	STD 6	8.780	3.952	20.246	5.881	9.376	48.924
10	STOCK STD	8.683	9.169	20.725	14.852	10.266	57.003
11	CHECK STD (sUB IN STOCK)	8.810	1.365	38.735	1.589	16.638	8.322
12	usgs	8.777	7.280	46.820	9.878	25.462	45.223
13	TAP	8.787	6.228	56.368	8.379	32.369	38.657
14	TAP	8.797	6.396	58.743	8.671	35.149	39.708
15	5	8.844	1.514	19.737	1.987	8.675	9.252
16	6	8.780	5.352	23.649	6.992	10.136	33.195
17	STOCK	8.677	11.204	22.696	16.559	10.845	69.703
18	CHECK	8.810	1.430	39.855	1.709	17.703	8.730
19	Q	8.767	0.462	1.094	0.932	0.425	2.690
20	PIN A JAN7	8.764	0.643	1.537	1.185	0.547	3.821
21	PAC A JAN 7	8.787	0.223	0.534	0.511	0.234	1.201
22	TUN A JAN7	8.787	0.134	0.323	0.322	0.147	0.649
23	MSH A JAN7	8.790	0.126	0.301	0.302	0.139	0.596
24	ICE A JAN7	8.777	0.467	1.135	0.965	0.445	2.722
25	ICE B JAN 7	8.787	0.513	1.235	1.041	0.479	3.009
26	PIN B JAN 7	8.794	0.597	1.419	1.166	0.546	3.532
27	PAC B JAN 7	8.834	0.216	0.500	0.496	0.225	1.156
28	TUN B JAN 7	8.830	0.242	0.568	0.552	0.254	1.322
29	MSH B JAN7	8.830	0.238	0.568	0.543	0.252	1.294
30	ICE B JAN 7	8.817	0.521	1.241	1.062	0.491	3.061
31	ICE A SEP95.2018	8.780	0.438	1.031	0.931	0.423	2.545
32	PAC A SEP5.2018	8.784	0.114	0.268	0.274	0.126	0.524
33	PIN A SEP5.2018	8.790	0.298	0.661	0.667	0.293	1.669
34	TUN A SEP5.2018	8.794	0.111	0.246	0.267	0.117	0.504
35	MSH A SEP5.2018	8.790	0.213	0.500	0.491	0.224	1.141

36	FRESHBASE	8.807	0.052	0.233	0.126	0.110	0.135
37	ICE B SEP 5. 2018	8.803	0.469	1.117	0.990	0.454	2.738
38	PAC B SEP 5.2018	8.830	0.113	0.258	0.270	0.122	0.514
39	PIN B SEP 5.2018	8.840	1.058	1.872	1.676	0.617	6.407
40	TUN B SEP5.2018	8.850	0.167	0.370	0.387	0.169	0.850
41	MSH B SEP5.2018	8.807	0.221	0.510	0.511	0.232	1.185
42	FRESH BASE 2	8.773	0.031	0.100	0.075	0.047	0.000
43	ICE A 7/19/2018	8.774	0.418	0.969	0.912	0.416	2.417
44	PAC A 7/19/2018	8.784	0.133	0.312	0.320	0.147	0.642
45	PIN A 7/19/2018	8.780	0.553	1.292	1.150	0.531	3.261
46	TUN A 7/19/2018	8.797	0.114	0.263	0.275	0.124	0.522
47	MSH A 7/19/2018	8.800	0.252	0.579	0.581	0.263	1.383
48	MIILIQ	8.810	0.036	36.353	0.087	19.314	0.035
49	ICE B 7/19/2018	8.797	0.484	1.123	1.036	0.473	2.830
50	PAC B 7/19/2018	8.817	0.223	0.511	0.515	0.233	1.200
51	PIN B 7/19/2018	8.807	0.396	0.781	0.875	0.342	2.281
52	TUN B 7/19/2018	8.750	0.258	0.595	0.598	0.269	1.417
53	MSH B 7/19/2018	8.767	0.301	0.676	0.689	0.303	1.685
54	FRESHBASE 3	8.787	0.026	0.074	0.063	0.035	-0.030
55	Q	8.780	0.012	0.563	0.028	0.621	-0.116
56	Q	n.a.	n.a.	n.a.	n.a.	n.a.	n.a.
57	Q	9.057	0.020	2.981	0.130	6.719	-0.066
58	Q	8.750	0.001	0.516	0.002	0.315	-0.184
59	Q	n.a.	n.a.	n.a.	n.a.	n.a.	n.a.
60	Q	n.a.	n.a.	n.a.	n.a.	n.a.	n.a.
61	Q	n.a.	n.a.	n.a.	n.a.	n.a.	n.a.
62	Q	n.a.	n.a.	n.a.	n.a.	n.a.	n.a.
63	Q	n.a.	n.a.	n.a.	n.a.	n.a.	n.a.
64	Q	n.a.	n.a.	n.a.	n.a.	n.a.	n.a.
65	Q	n.a.	n.a.	n.a.	n.a.	n.a.	n.a.
66	Q	n.a.	n.a.	n.a.	n.a.	n.a.	n.a.
67	Q	n.a.	n.a.	n.a.	n.a.	n.a.	n.a.
68	Q	n.a.	n.a.	n.a.	n.a.	n.a.	n.a.
69	Q	n.a.	n.a.	n.a.	n.a.	n.a.	n.a.
70	Q	n.a.	n.a.	n.a.	n.a.	n.a.	n.a.
71	Q	n.a.	n.a.	n.a.	n.a.	n.a.	n.a.
	Sum:	501.056	68.180	724.010	104.225	482.065	681.678
	Average:	8.790	1.196	12.702	1.829	8.457	11.959
	Rel.Std.Dev:	0.568 %	200.027 %	164.217 %	188.545 %	196.475 %	163.452 %